KATHMANDU UNIVERSITY

SCHOOL OF ENGINEERING

DEPARTMENT OF MECHANICAL ENGINEERING

PROJECT REPORT ON

"COMPUTATIONAL AND EXPERIMENTAL STUDY OF FLOW OVER MULTI-ELEMENT AIRFOIL"

In Partial Fulfillment of the Requirements for the Bachelor's Degree in Mechanical Engineering

AUTHORS

SUNIL BELBASE [41088]

AAKASH MALI [41103]

SUJIT MAN SHRESTHA [41113]

May 2023

This report is intended for students and engineers who are willing to study about airfoils, single or inclusive of multiple elements. This report is fluid mechanics intensive and presents necessary information to introduce the readers on basics of multi-element airfoil and its flow visualization using different techniques popular in fluid mechanics. Necessary referencing for further studies is permitted.

AUTHORIZATION

We hereby declare that we are the authors of this project entitled “COMPUTATIONAL AND EXPERIMENTAL STUDY OF FLOW OVER MULTI-ELEMENT AIRFOIL”.

SUNIL BELBASE

AAKASH MALI

SUJIT MAN SHRESTHA

May 2023

PROJECT EVALUATION

"COMPUTATIONAL AND EXPERIMENTAL STUDY OF FLOW OVER MULTI-ELEMENT AIRFOIL"

by

Sunil Belbase
Aakash Mali
Sujit Man Shrestha

This is to certify that I have examined the document and have found that it is complete and satisfactory in all respects, and that any and all revisions required by the thesis examination committee have been made.

_____

Assist. Prof. Dr SAILESH CHITRAKAR
(Project Supervisor)

_____

Assist. Prof. Mr. CHIRANJEEVI MAHAT
(Project Co-Ordinator)

_____

(External Examiner)

May 2023

ACKNOWLEDGEMENT

We would like to thank everyone who has helped us conduct this project. We would like to express our special thanks to our project supervisor **Dr Sailesh Chitrakar**, who has supervised us throughout two consecutive projects. His help, suggestions, support and encouragement has helped us accomplish the objectives of our research. Many thanks to the Department of Mechanical Engineering, **KATHMANDU UNIVERSITY** for providing us the opportunity to work on marvelous projects as this one. And we would like to express our gratitude among everyone who involved in this project directly or indirectly.

Our special thanks go to countless readers of this report who provide us with important comments and further suggestions to improve our existing project. We welcome constructive comments and suggestions which will help us to do better in future.

It is our radiant sentiment to place on record our kindest regards to whoever were directly and/or indirectly involved in the successful completion of this project computationally and experimentally. We would also like to acknowledge the presence of Fablab Nepal, Pulchowk, Lalitpur. Fablab has provided us necessary supports and space for fabrication of the multi-element airfoil on which the entire study was performed.

Table of Contents

Chapter 1 Introduction 1

1.1 Understanding Airfoil Basics 1

1.2 Introduction to Multi-Element Airfoils 3

1.3 Scope of Study 6

1.4 Aims of Study 6

Chapter 2 Literature Review 7

2.1 Aerodynamic Analysis of Aircraft Wing 7

2.2 Kutta-Joukowski Theorem 11

2.3 Potential Flow Theory 12

2.4 Vortices 14

2.5 Important Aerodynamic Theories 15

2.5.1 Boundary Layer Theory 15

2.5.2 Lifting Line Theory 15

2.5.3 Thin-Airfoil Theory 16

2.6 Types of Airfoils and Airfoil Geometry 16

2.7 Concerned Airfoil Profiles 19

2.7.1 Clark Y Airfoils 19

2.7.2 NACA Airfoils 20

2.8 Flow Visualization Techniques 21

2.8.1 Smoke Flow Visualization Method 21

2.8.2 Tuft Flow Visualization Method 22

2.8.3 Digital Particle Image Velocimetry 22

Chapter 3 Investigation of Airfoil Geometry and Working Methodology 23

3.1 Multi-Element Wing Geometry 23

3.2 Double-Element Profile Orientations 24

3.2.1 Profile 1: With upper flap 24

3.2.2 Profile 2: With lower flap 24

3.2.3 Profile 3: With upper slat 24
3.2.4 Profile 4: With lower slat 25
3.3 Methodology Blueprint 25
3.4 Dimensional Analysis and Modeling 26
3.5 Dimensional Irrelevance 26
3.6 Output Visualization Methodology 28
3.6.1 C_p vs x/c Graph 28
3.6.2 C_L vs Re Plot 31
Chapter 4 Computational Setup, Results and Discussions 32
4.1 Simulation Setup 32
4.1.1 About ANSYS 32
4.1.2 Standardized Simulation Parameters 32
4.1.3 Turbulence Modeling Methods 33
4.1.4 Solution Algorithms 34
4.2 Simulation Results Approach 1: Unbroken Geometry 35
4.2.1 Single-Element Profile 35
4.2.2 Double-Element Profile 1 at 0 degrees AOA 37
4.2.3 Double Element Profile 2 at 0 degrees AOA 38
4.2.4 Double Element Profile 3 at 0 degrees AOA 39
4.2.5 Double Element Profile 4 at 0 degrees AOA 40
4.2.6 Double Element Profile 4 at 5 degrees Flap AOA 41
4.2.7 Double Element Profile 4 at 10 degrees Flap AOA 43
4.2.8 Double Element Profile 4 at 15 degrees Flap AOA 44
Chapter 5 Experimentation Setup 45
5.1 Fabrication of Double Element Clark Y Airfoil 45
5.2 Edibon EEE Wind Tunnel Setup 46
5.3 Scan valve Pressure Transducer 48
5.4 Instrument Error 50
5.5 Tuft Airflow Visualization 52

Chapter 6 Experimentation Results and Validation 53
6.1 Summary and Instrument error 53
6.2 Pressure Taps Over Airfoil Surfaces 53
6.3 Pressure Readings and Data Tables 55
6.3.1 For 0 degrees Flap AOA 55
6.3.2 For 5 degrees Flap AOA 57
6.3.3 For 10 degrees Flap AOA 59
6.3.4 For 15 degrees Flap AOA 61
6.4 Validation from Tufts 63
6.4.1 Front element at -5° AOA, Back element at 15° AOA at speed of 4m/s 63
6.4.2 Front element at 0 degrees AOA, back element at 5 degrees AOA at 4m/s 64
6.4.3 Front element at 0 degrees AOA, back element at 5 degrees AOA at 8m/s 64
6.4.4 Front element -5° AOA, Back element at 15° AOA at speed of 8m/s 64
6.4.5 Front element at 15° AOA, Back element at 15° AOA at speed of 8m/s 65
Chapter 7 Conclusion 66
Glossary: Flight Mechanics 67
Glossary: ANSYS and Computational Fluid Dynamics 69

List of figures

Fig 1: Symmetric vs Asymmetric airfoil geometry 1
Fig 2: Terminologies of an airfoil geometry 2
Fig 3: Flow separation around an airfoil causing pressure drag.....3
Fig 4: Depiction of multi-element airfoil 4
Fig 5: Airflow around a three-element airfoil. Openings on the surface of multi-element airfoils act as passage for air to flow through hence compensating flow separation through flow recirculation.....5
Fig 6: McDonnell Douglas aerospace multi-element airfoil 5
Fig 7: Airfoil section of a wing.....7
Fig 8: Pressure coefficient (Cp) vs chord length (x/c) that shows increased static pressure of air as it nears the trailing edge and representing adverse pressure gradient 8
Fig 9: Viscous shear stresses and normal pressure stresses in a fluid element 8
Fig 10: Pressure distribution around airfoil surface that shows higher suction pressure on top 9
Fig 11: Superposition of idealized uniform irrotational flow and circulatory flow 10
Fig 12: Net vorticity in the flow domain is zero.....14
Fig 13 An unrealistic lift distribution that neglects three-dimensional effects vs a realistic span-wise trapezoidal lift distribution observed over a finite wing.....16
Fig 14: Trailing edge vortices formed by span-wise change in lift distribution.....16
Fig 15: Airfoil geometry: 1: Zero-lift line; 2: Leading edge; 3: Nose circle; 4: Max. thickness; 5: Camber; 6: Upper surface; 7: Trailing edge; 8: Camber mean-line; 9: Lower surface 17
Fig 16: Different airfoil geometries from around early 1900s 18
Fig 17: Early airfoil geometries with different range of Reynolds number 18
Fig 18: Clark Y airfoil at zero AOA.....20
Fig 19: Different NACA airfoil profiles.....20
Fig 20: Smoke visualization technique used in an airfoil to visualize laminar flow, turbulent flow, boundary layer separation and vortices around airfoil 21
Fig 21: Tuft Visualization method to visualize boundary separation.....22
Fig 22: Two element Clark-Y airfoil with a gap of 5mm and overlap of 6mm constructed using Solidworks 2D. Dimensions are explained in section 2.3.....23
Fig 23: Double element orientation with flap above the trailing edge of main element 24
Fig 24: Double element orientation with flap below the trailing edge of main element.....24

Fig 25: Double element orientation with slat above the leading edge of main element 24
Fig 26: Double element orientation with slat below the leading edge of main element 25
Fig 27: Velocity distribution contour for Clark Y airfoil 35
Fig 28: Pressure distribution contour for Clark Y airfoil 36
Fig 29: Graph representing Pressure coefficient as a function of distance 36
Fig 30: Pressure and Velocity distribution contour for profile 1.....37
Fig 31: Pressure and Velocity distribution contour for profile 2.....38
Fig 32: Pressure and Velocity distribution contour for profile 3.....39
Fig 33: Pressure and Velocity distribution contour for profile 4 in grayscale.....40
Fig 34: Pressure and Velocity distribution contour for profile 4 at 5 degrees of flap AOA ...42
Fig 35: Pressure and Velocity distribution contour for profile 4 at 10 degrees of flap AOA .43
Fig 36: Pressure and Velocity distribution contour for profile 4 at 15 degrees of flap AOA .44
Fig 37: Layer wise manufacture of airfoil profiles using automated CNC 45
Fig 38: Final double-element airfoil system with 3 degrees of freedom.....46
Fig 39: Edibon wind tunnel setup available at ESTRL, Kathmandu University.....47
Fig 40: Channel pressure scanner, model no. DSA3207 48
Fig 41: Deviation of values of same static pressure as a result of instrumental error for different velocities 51
Fig 42: Placement of tufts at distances relative to the leading edge of the airfoil system.....52
Fig 43: Taps at different locations relative to leading edge of the airfoil system 53
Fig 44: Graph of Cp vs tap position for 0 degrees flap AOA.....56
Fig 45: Graph of Cp vs tap position for 5 degrees flap AOA.....58
Fig 46: Graph of Cp vs tap position for 5 degrees flap AOA.....60
Fig 47: Graph of Cp vs tap position for 5 degrees flap AOA.....62
Fig 48: Tufts and its positions 63
Fig 49: Wiggling tufts representing boundary separation 63
Fig 50: Tuft visualization of attached flow to some extent 64

ABSTRACT

This report provides a comprehensive guide to understanding multi-element airfoils at velocities as low as 8m/s and presents a computational and experimental study summary of double-element airfoils. Study was done on the unbroken geometries of Clark Y airfoil stacked one after another with a gap of 5mm and overhang of 6mm. The main objectives of the study were to investigate flow field generated by double-element airfoils at different orientations and to visualize flow around multiple elements through simulation and validate them using different experimental approaches such as pressure tapping for quantitative authentication and tuft flow visualization for qualitative justification. Simulations were performed on different orientations and AOAs of the flap element and a promising orientation was selected for further experimental studies, which in the end indicated stall behavior of the airfoil system on AOA of flap greater than 5 degrees.

List of Abbreviations/Symbols

g	Acceleration due to gravity
AOA, α	Angle of Attack
P_∞	Atmospheric pressure
c	Chord length of airfoil
c_f	Chord length of flap
c_m	Chord of main element
C_L	Coefficient of lift
C_D	Coefficient of drag
ρ	Density of fluid
x	Distance of streamwise component from front stagnation point
ν	Kinematic viscosity
M	Mach number
C_p	Pressure coefficient
Re	Reynolds number
C_f	Skin friction coefficient
P_0	Stagnation pressure
ε	Turbulence dissipation rate
u, v, w	Velocity components

Chapter 1 Introduction

1.1 Understanding Airfoil Basics

An airfoil is a streamlined structure that has the ability to generate a significant amount of lift. Airfoils generate lift force based on the principle of Bernoulli, where difference in the flow velocity results in creation of pressure difference below and above the structure. Airfoil design is a major facet of aerodynamics. Various airfoils serve different flight schemes and patterns. There are symmetric airfoils and there are asymmetric airfoils, both with distinct characteristics. But the basic requirement of an airfoil is to have an asymmetric geometry. Asymmetric airfoils can generate lift at zero angle of attack, while a symmetric airfoil may better suit for frequent inverted flights as in an aerobatic airplane. Such symmetric airfoils may be required to be placed at a certain angle (called as angle of attack) in order to create a pressure difference.

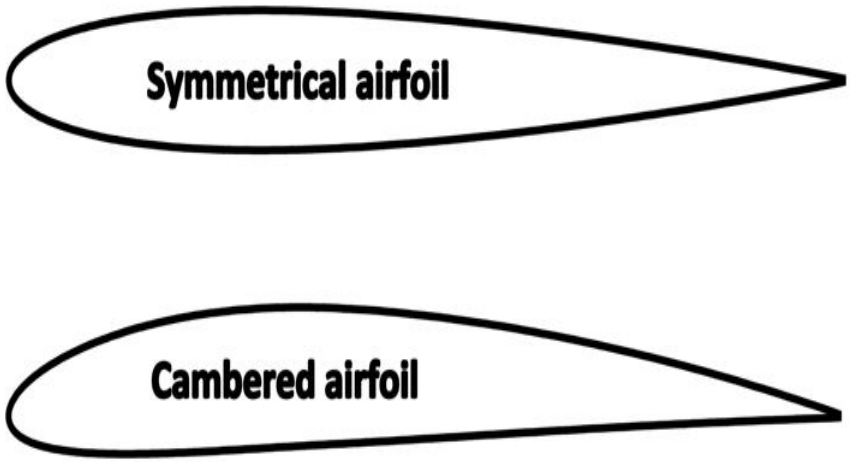

Fig 1: Symmetric vs Asymmetric airfoil geometry

The resurgence of lift aerodynamics and innovation in wing designs have been significant results of work done in the aircraft industry over the past ten years to improve cruise wing efficiency. In comparison to earlier generation designs, new-generation wing concepts may have smaller wing areas, higher aspect ratios, and thinner wings [1].

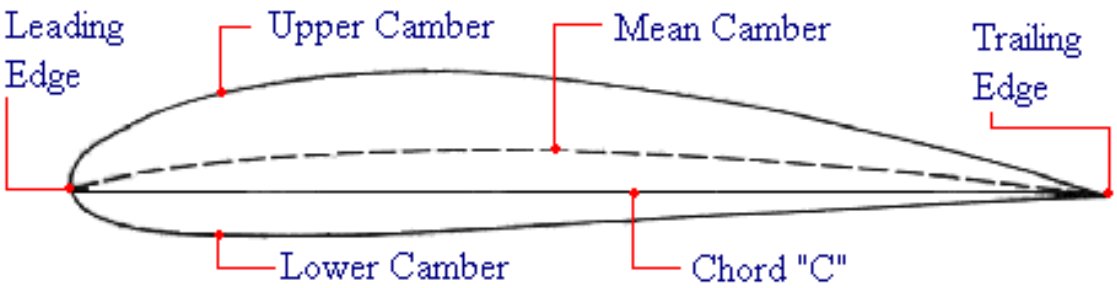

Fig 2: Terminologies of an airfoil geometry

An airfoil works on the basis of Bernoulli's principle.

$$\frac{P}{\rho} + \frac{v^2}{2} + gz = Constant$$ ----------**(Equation 1)**

The upper surface of the wing is highly curved in comparison with the bottom surface curve. This allows the free stream flow of air on the upper surface to travel more distance than on the bottom surface, thus raising the velocity of the free stream on the upper side than on the lower side. From equation (1), increase in velocity tends to decrease static pressure of the fluid. The overall structure of the airfoil is asymmetric in nature in order to enhance this pressure difference above and below. However symmetric structure is also preferred in a few cases. A normal airfoil works fine within the domain of subsonic flow. Theoretical efficiency and practically obtained efficiency tend to match except for certain errors caused due to surface roughness. However, when the airfoil is exposed under sonic or flows at higher Mach numbers, the flow separation becomes a significant issue and major cause for pressure drag that reduces the theoretical efficiency of structure.

$$F_d = \frac{1}{2} C_d A v^2$$ ----------**(Equation 2)**

Equation 2 gives the basis for determining the drag force associated with any cross section 'A' subjected at the flow velocity 'v'. Hence, the idea of multi element structure is introduced in order to reduce or eliminate the flow separation. The openings allow a certain portion of high-pressure flow to run into low pressure zones. The flow compensates for the vacuum that would otherwise cause pressure drag.

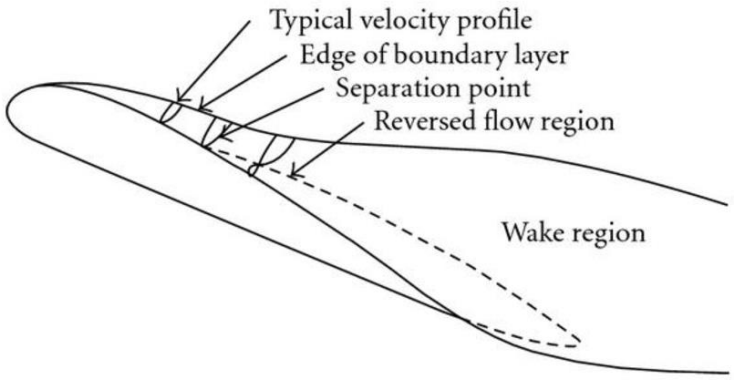

Fig 3: Flow separation around an airfoil causing pressure drag

1.2 Introduction to Multi-Element Airfoils

A multi-element airfoil is an aircraft wing design that consists of multiple wing sections or elements, rather than a single continuous surface. These elements may be mounted one behind the other, or they may be mounted at different locations along the span of the wing. Multi-element airfoils can be used to improve the performance of an aircraft in various ways. For example, they can be used to increase the lift of the wing at a given angle of attack, or to reduce drag by delaying the separation of the boundary layer on the wing surface. They can also be used to control the wing's pitch and roll stability, or to optimize the wing's performance at different speeds and altitudes.

A multi-element airfoil typically consists of a main wing and several leading- and trailing-edge components. A very efficient way to raise an aerodynamic system's maximum lift is to use multi-element wings. The complexity and weight of the high-lift systems are being reduced through the design of aircraft. The multi-element system for the wings was introduced in this way, and it is still true today. Figure 4 depicts the multi element wings [2]. Multi-element wings are essentially used to produce more down force. A single element wing is unable to produce as much force as a multi element wing. This is due to the capability of multi-element wings to account for flow separation and avoid pressure drag losses. The number of elements that make up a multi-element wing allows for further classification [3]. Depending on the application, the multi-element airfoil may have two, three, four, five, or more elements. Although more lift is produced as the number of wing elements increases, there is also a corresponding rise in drag. The cross-sectional area exposed to the flow determines the drag force directly.

Since the planform area of multi element wings are greater than that of a single element airfoil, the drag and lift produced by these wings are also more significant. Even at low angles-of-attack, separation of flow in airfoils can happen. This complex phenomenon depends on geometry and flight conditions. Typically, separation issues manifest on the flap, particularly in single flap configurations. Vortex generators mounted on flaps can enhance performance significantly [4]. The lift force applied to the structure is increased by the multiple elements' larger cross sections, though.

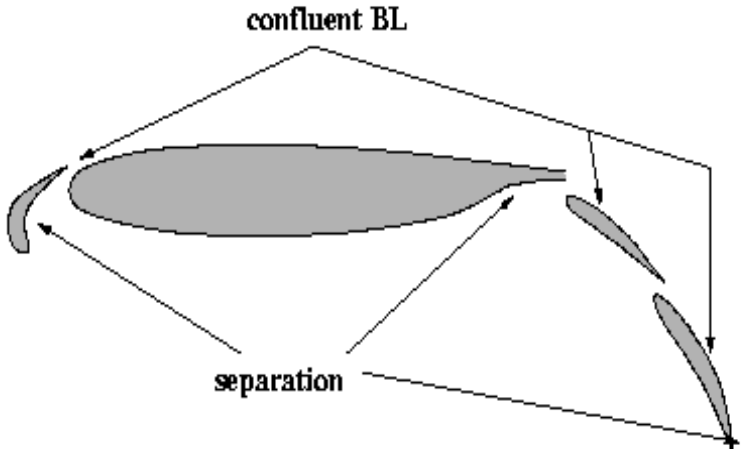

Fig 4: Depiction of multi-element airfoil

Multi-element wings exhibit a variety of flow phenomena, such as wakes from upstream elements combining with new boundary layers on downstream elements, flow separation in cove regions, flow separation on the downstream elements, especially at high angles (landing configurations), confluent boundary layers, high-curvature wakes, high flow deflection, and possibly supercritical flow in the upstream elements [5]. When two boundary layers grow on different solid surfaces and merge, they are said to be confluent (generally at a different stage of development). The local velocity field can be used to locate confluent boundary layers. Cove regions experience flow separation due to the high curvature and locally high speed. In aircraft configurations, supercritical regimes may also be caused by high speed.

The maximum lift that a single or multi-element wing (or more complex devices) can achieve is typically attributed to flow separation on the suction side and on the maximum suction peak. The two issues are somewhat interrelated. Camber and thickness distributions, surface quality, leading edge radius, and trailing edge angle are among the airfoil characteristics that have a significant impact on the maximum lift coefficient. Maximum lift coefficient is also influenced

by Reynolds number. The operation on the aforementioned parameters must, among other things, delay the pressure recovery on the suction side and remove or postpone the flow separation at a fixed Reynolds number. Figure 5 represents airflow pattern around a three-element airfoil.

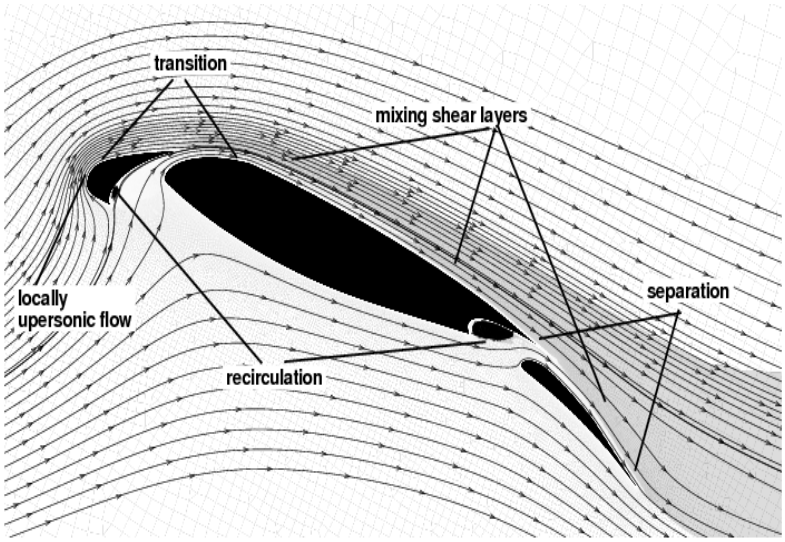

Fig 5: Airflow around a three-element airfoil. Openings on the surface of multi-element airfoils act as passage for air to flow through hence compensating flow separation through flow recirculation

There are several types of multi-element airfoils, including slats, flaps, and spoilers. Slats are movable leading-edge devices that extend forward from the wing to increase lift at low speeds. Flaps are hinged devices that can be extended downward from the rear of the wing to increase lift and drag, and are often used during takeoff and landing. Spoilers are devices that can be extended upward from the wing surface to disrupt the flow of air over the wing and reduce lift, and are often used to control the descent rate of an aircraft during landing.

Numerical results show that the aerodynamic parameters of multi element airfoils with tail effect is much optimum than the standard NACA airfoils. [5]

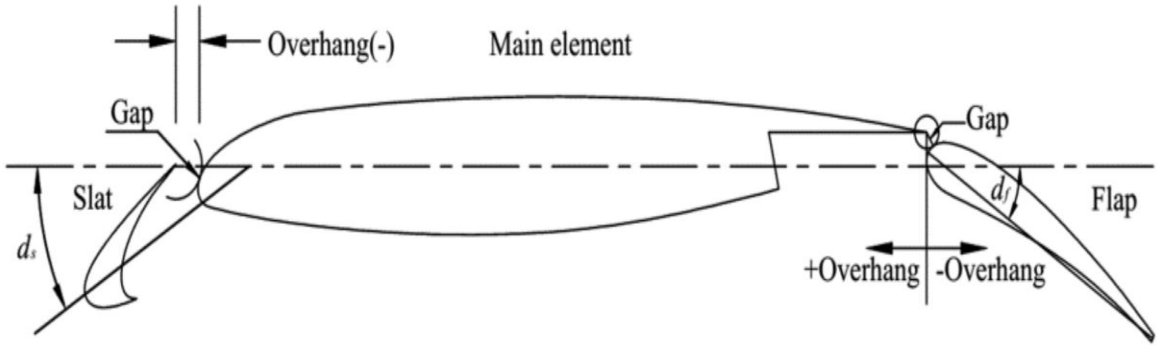

Fig 6: McDonnell Douglas aerospace multi-element airfoil

1.3 Scope of Study

The topic of high-lift wings is one which currently attracts significant research. In race cars, where enormous amounts of downforce are required to improve cornering capabilities, multi element wings are used. Multi-element airfoils are also used by airplanes as wing flaps in addition to race cars. With the ability to retract during high-altitude cruising, these adjustable flaps enable the planes to produce a greater magnitude of lift force during takeoff and landing periods [5]. Multi-element airfoils and their behaviors have been studied throughout the world, further enhanced by the research for application in race cars through computational analyses, modeling, and experimentations. The majority of these behavioral studies have been performed for subsonic flows, but no significant studies have been performed on supersonic and hypersonic flows, or in the field of aerospace, where there could be possibility of completely replacing single element airfoils with multi-elements in specific cases.

A multi-element wing in ground effect considers downforce, while an inverted form of the same might be considered for high lift applications where adverse pressure gradient is imposed. Therefore, insights into the lift enhancing and lift limiting mechanisms may be gained from this study. Hence another application of this study could be aerial vehicles cruising at varying speeds.

With the aid of this study, the overall performance of a particular airfoil can be compared with an equivalent multi-element airfoil. Basis of comparison could be set through same projection area, camber length and chord length for both the wings so that effect of both single and multi-element airfoils remain equivalent. The methodology is further discussed in upcoming sections.

1.4 Aims of Study

The general objectives of this research are as follows:

- To investigate flow field generated by double-element airfoils at different orientations
- To visualize flow around multiple elements

The specific aim of this research is as follow

- To measure overall C_L as a function of flow velocity for given double-element airfoil

Chapter 2 Literature Review

2.1 Aerodynamic Analysis of Aircraft Wing

Aerodynamic issues can arise from the way air interacts with a solid body moving through it, such as an airplane wing. Aerodynamic researchers are interested in the best shapes for an airfoil to give a wing the most lift and the least drag during takeoff and flight.

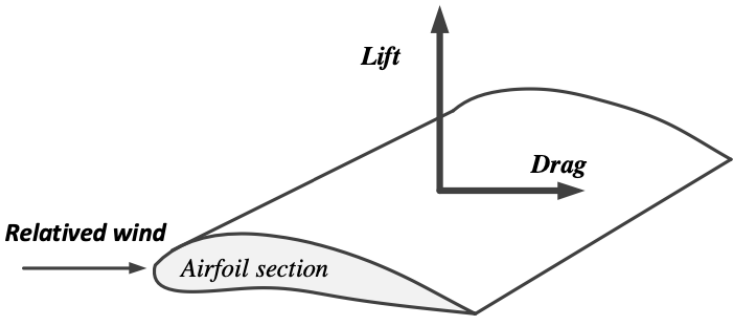

Fig 7: Airfoil section of a wing

Lift is the force that holds an aircraft in the air while directly opposing the weight of the aircraft. This force is perpendicular to the flow direction and acts through the object's center of pressure. The flow turning theory is used to show how airflow around the airfoil produces lift. The geometry of the airfoil, the viscosity of the airflow, and the Coanda effect cause the airflow to pass over the upper surface and create a vertical airflow past the trailing edge. Lift is produced when a low-pressure system develops over an airfoil. [4]

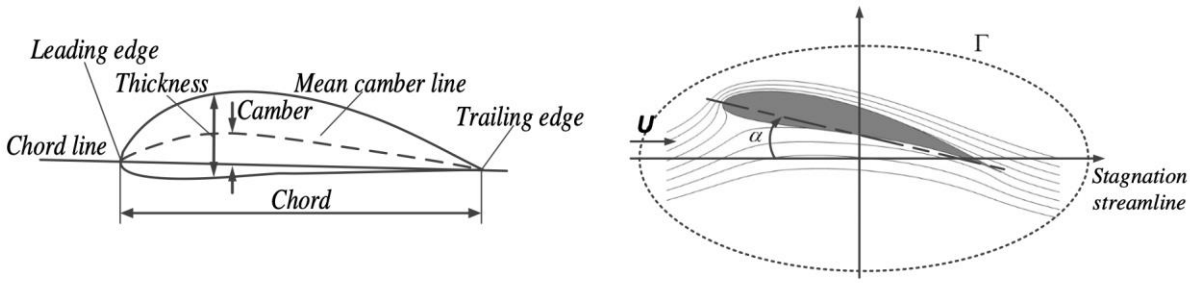

Generally, lift and drag forces in an airfoil are associated with two kinds of stresses: Normal pressure stresses (tau) and Viscous shear stresses (sigma) respectively. Hence, lift force acting on an airfoil is due to the difference in pressure field distributed around it.

Adverse Pressure Gradient: Adverse Pressure gradient can be considered as the pressure difference between upwash and downwash stream of air that causes the air velocity to reduce. Eventually, the velocity of the boundary layer goes to zero and detaches from the surface. The layer where the viscous force is significant is called the boundary layer.

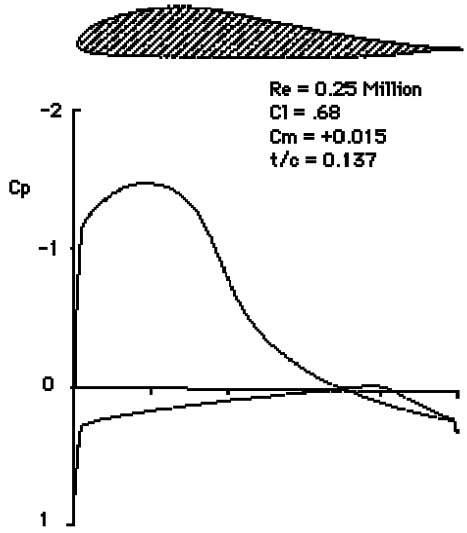

Fig 8: Pressure coefficient (Cp) vs chord length (x/c) that shows increased static pressure of air as it nears the trailing edge and representing adverse pressure gradient

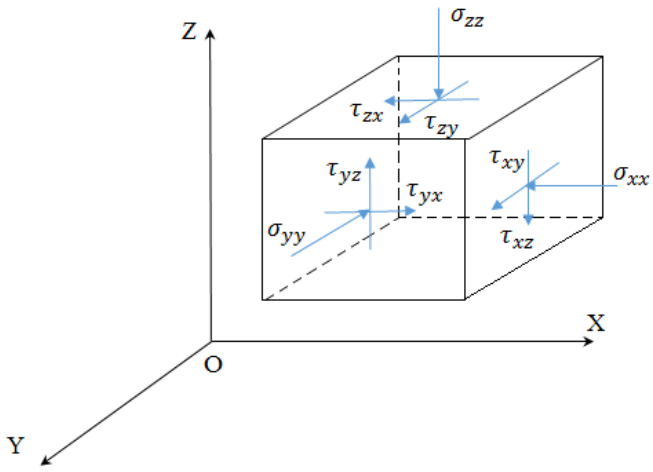

Fig 9: Viscous shear stresses and normal pressure stresses in a fluid element

This casualty of pressure and velocity gradient is given by Bernoulli's theorem from Equation 1. But the exact cause of presence of velocity gradient in the first place is studied less. One explanation is that the geometry causes the flow to be pinched together above the airfoil, but not below it. And by virtue of mass conservation, higher velocity is obtained at upwash. [25]

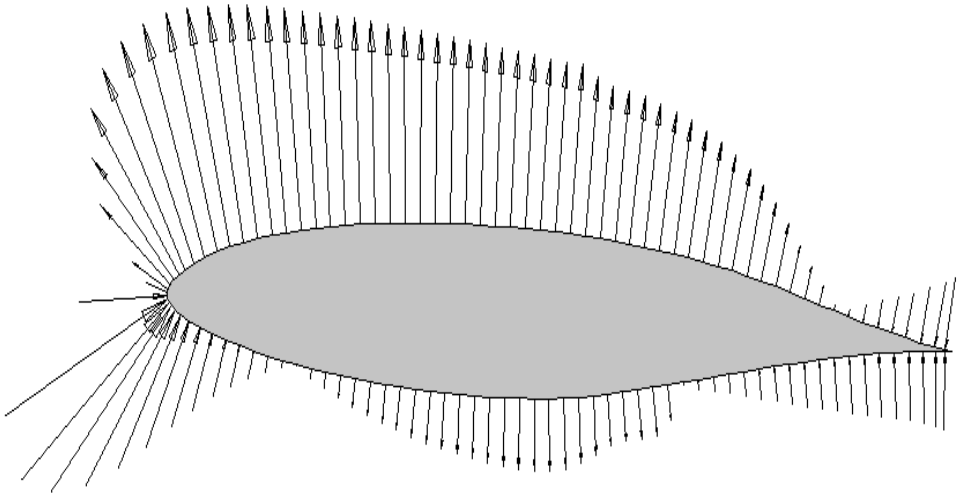

Fig 10: Pressure distribution around airfoil surface that shows higher suction pressure on top

A more complete but less intuitive explanation for the difference in velocity is based on the concept of circulation. Circulation is the total vorticity within a given closed loop. If a closed loop is drawn from leading edge to trailing edge at a given span location, the total vorticity passing through this loop is the circulation of the given span location. Circulation is a mathematical concept used to explain the motion of air from a frame of reference bound to the wing and thus, in reality, no molecule revolves around the airfoil.

The flow around an airfoil can be thought of as the superposition of idealized uniform irrotational flow (parallel flow layers), and circulatory flow. The flow above the airfoil is accelerated by circulation, while the flow at bottom is delayed [26].

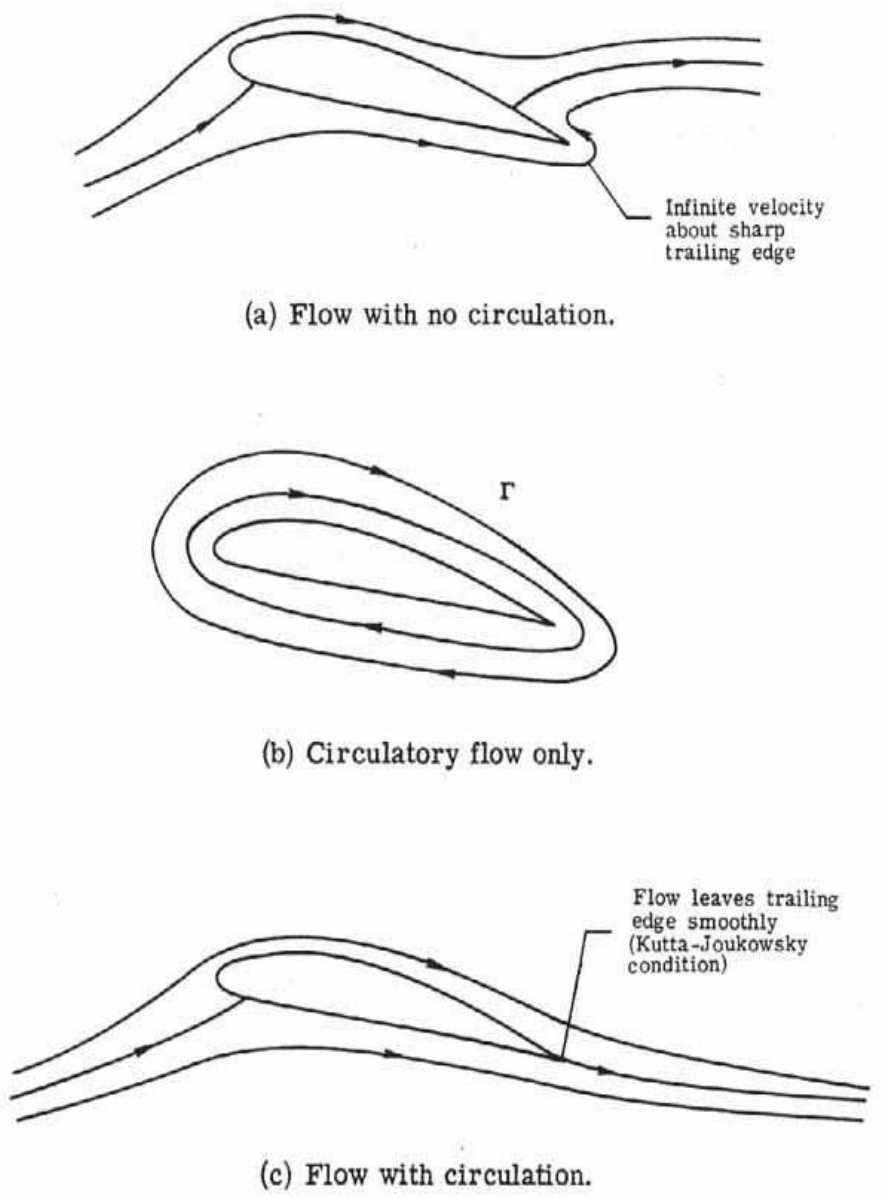

Fig 11: Superposition of idealized uniform irrotational flow and circulatory flow

If a condition is imposed for requirement of parallel flow at the trailing edge, circulation that the airfoil must generate can be calculated. This condition is called Kutta-Joukowski condition

2.2 Kutta-Joukowski Theorem

From Kutta-Joukowski theorem, lifting force for an airfoil with round leading and sharp trailing edge immersed in a uniform stream with an effective angle of attack, proportional to the density of air ρ, relative velocity of the airflow *U* and the circulation Γ generated by the bound vortex. In fluid dynamics, the lift per unit span (L') acting on a body in a two-dimensional flow field is directly proportional to the circulation, i.e., it can be expressed as the product of the circulation Γ about the body, the fluid density *ρ*, and the speed of the body relative to the free-stream **v.** The lifting force *L* acting on the airfoil is defined as:

$$L = \rho v \Gamma$$ ----------**Equation 3**

where $\Gamma = \int u.dl$ is circulation around the wing.

A lift-producing airfoil either has camber or operates at a positive angle of attack, the angle between the chord line and the fluid flow far upstream of the airfoil. Moreover, the airfoil must have a sharp trailing edge. Any real fluid is viscous, which implies that the fluid velocity vanishes on the airfoil. Prandtl showed that for large Reynolds number, defined as

$$\mathrm{Re} = \frac{\rho V_\infty c_A}{\mu}$$ ----------**Equation 4**

and small angle of attack, the flow around a thin airfoil is composed of a narrow viscous region called the boundary layer near the body and an inviscid flow region outside. In applying the Kutta-Joukowski theorem, the loop must be chosen outside this boundary layer. (For example, the circulation calculated using the loop corresponding to the surface of the airfoil would be zero for a viscous fluid.)

The sharp trailing edge requirement corresponds physically to a flow in which the fluid moving along the lower and upper surfaces of the airfoil meet smoothly, with no fluid moving around the trailing edge of the airfoil. This is known as the *Kutta condition*.

Kutta and Joukowski showed that for computing the pressure and lift of a thin airfoil for flow at large Reynolds number and small angle of attack, the flow can be assumed inviscid in the entire region outside the airfoil provided the Kutta condition is imposed. This is known as the potential flow theory and works remarkably well in practice.

If the effective angle of attack is α, the length of the wing l, and the chord length of the airfoil is c, with the Joukowski transformation the magnitude of the circulation is found as

$$\Gamma = \pi \alpha c v l$$ ----------**Equation 5**

Substituting the value of Γ into Eq. 1 gives the sectional lift force as:

$$L = \pi\alpha\rho clU2 = 1/2 Cl\rho SU^2$$ ----------**Equation 6**

where $C_L = 2\pi\alpha$ is called the coefficient of lift, S = c*l is the area of the airfoil as viewed from an overhead perspective.

The other aerodynamic force that affects an airfoil and is perpendicular to the lifting force, is called drag. This force opposes the relative motion of the airfoil and has direction parallel to the airflow because skin friction drag appears between the air molecules and the surface of the airfoil. Similarly, the expression for calculating the drag of airfoil is defined as/ as follows:

$$D = 1/2\ C\ D\ \rho\ A\ U^2$$ ----------**Equation 7**

where *D* is the drag force, *A* is a reference area, and *CD* is the drag coefficient.

In summary, aerodynamic forces of the airfoil depend on the shape of the airfoil, the density, viscosity and compressibility of the air, and the wing surface area and angle of attack. Lift coefficient and drag coefficient are two dimensionless coefficients that are associated with the aerodynamic forces. From Eq. 2 and Eq. 3, these coefficients are determined through velocity of the moving body, density and velocity of the airstream, and the corresponding reference area.

2.3 Potential Flow Theory

It is reasonable to assume that external flows around bodies are inviscid and irrotational. This is due to the fact that the boundary layer, a thin layer next to the body surface, is where the viscous effects are restricted. The boundary layer can be defined using a continuous function that complies with the fundamental principles of fluid mechanics: the conservation of mass and momentum and the assumption of an incompressible, inviscid, and irrotational flow.

Potential flow, also known as velocity potential, is the term used in fluid dynamics to describe the velocity field as the gradient of a scalar function. As a result, an irrotational velocity field, which is a useful approximation for many applications, characterizes a potential flow. The potential flow approximation is not applicable for flows with significant vorticity effects. Hence by definition, if the curl of a vector is zero, the vector can be expressed as the gradient

of a scalar function Φ=Φ(x,y,z), called the potential function. In case of fluid dynamics, vector v is the velocity vector, the curl of which is the vorticity vector ζ, and thus Φ is called Velocity Potential function, such that, for irrotational regions of flow,

$$v = \nabla . \Phi$$

And since the curl of a gradient is zero, $\nabla \times \nabla . \Phi = 0$

$$\therefore \nabla \times v = 0$$

The curl of the velocity field is zero for irrotationality. Furthermore, for Navier-Stokes Continuity equation

$$\nabla . v = 0$$

$$\nabla . \nabla . \Phi = 0$$

$$\therefore \nabla^2 . \Phi = 0 \text{ ----------Equation 8}$$

Irrotational flow regions are also known as potential flow regions. This approximation reduces the number of equations that must be solved analytically by combining three unknown velocity components—u, v, and w—into one unknown scalar variable. With the given set of boundary conditions surrounding the entire irrotational region of the flow field, equation 3 can be solved regardless of the fluid properties. Once Φ has been calculated, ∇ can also be calculated everywhere in that region of flow field, without ever having to solve Navier-stokes equation. The solution is valid for any incompressible fluid, regardless of its density or its viscosity, in regions of the flow in which irrotational approximation is valid.

2.4 Vortices

In three-dimensional flows, boundary layer separation causes the viscous flow sheet, which was previously contained in a thin layer attached to the wall, to roll up and suddenly jump into the outside non-dissipative flow. These vortical formations are usually referred to as vortices. Such vortices frequently dominate the overall flow parameters and can be seen in a wide variety of situations. A surface accelerating through a fluid medium resists flow through shear stresses which are associated with the viscosity of the fluid, i.e. the shear stresses tend to rotate fluid elements, thus creating vortices. This twisting phenomenon is called vorticity which measures the rate of local fluid rotation, and the surfaces are regarded as vortex sources. Equation 3 defines the vorticity. In fluid mechanics, Helmholtz's theorems describe three-dimensional motion of fluid in the vicinity of vortex lines/vortex filaments. These theorems apply to inviscid flows and are stated as follows

- The strength of vortex line is constant along its length
- A vortex line cannot end in a fluid
- A fluid element that is initially irrotational remains irrotational

Types of Vortices

- Starting vortex: Forms in the air adjacent to the trailing edge of an airfoil as it is accelerated from rest
- Horseshoe vortex: A vortex system modeled by a bound vortex attached to a wing along with two trailing vortices that resembles a horseshoe.
- Wingtip vortex: Wingtip vortices are circular patterns of rotating air left behind a wing as it generates lift. Wingtip vortices trail from the tip of the wing.
- Bound Vortex: The flow rotation that occurs on the surface of airfoil as it accelerates
- Shed vortex: Vortices that are formed from the trailing edge and detach periodically.

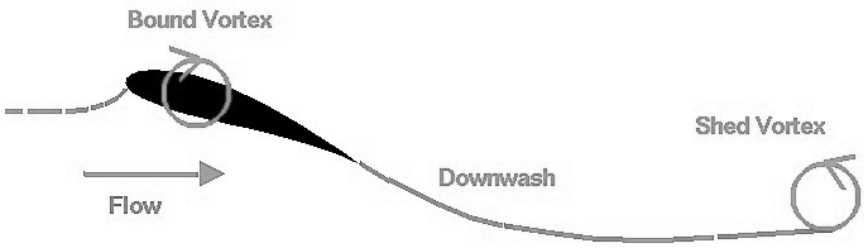

Fig 12: Net vorticity in the flow domain is zero

2.5 Important Aerodynamic Theories

2.5.1 Boundary Layer Theory

This theory was published by Professor Ludwig Prandtl of Germany in 1904 [20]. According to the boundary layer theory, liquid particles adjacent to a moving fluid adhere to it. The reason an object senses friction drags or vice versa is because the actual fluid phenomena are constrained by the boundary layer. In aerodynamics, the boundary layer is important because it essentially alters the airfoil's shape. Laminar flow is created when the boundary layer flow is attached to the airfoil surface at lower angles of attack. Separated flow is created when the boundary layer flow is separated from the airfoil surface at high angles of attack.

2.5.2 Lifting Line Theory

The entire amount of lift that a wing of a given geometry will produce is challenging to determine analytically. The first step in comprehending a three-dimensional finite wing is to imagine cutting it into cross-sections and studying each one separately as a wing in a two-dimensional environment. An airfoil is the name given to each of these slices, and it is simpler to comprehend an airfoil than a full three-dimensional wing. One would assume that interpreting the lift over the entire wing would only require adding the separately determined forces from each airfoil segment. The lift over each wing segment (local lift per unit span) on a real wing does not simply correspond to what two-dimensional analysis predicts, proving that this approximation is wildly inaccurate. In actuality, adjacent wing sections have a significant impact on the local amount of lift on each cross-section.

By considering some of the interactions between the wing slices, the lifting-line theory corrects some of the flaws in the simplistic two-dimensional method. Based on the wing geometry (span-wise distribution of chord, airfoil, and twist) and flow conditions, it generates the lift distribution along the span-wise direction [27].

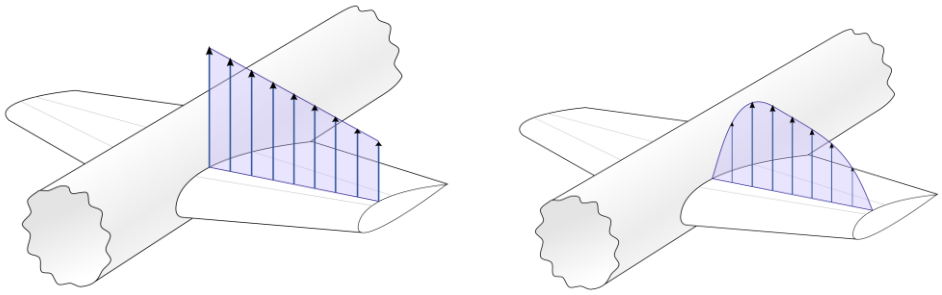

Fig 13 An unrealistic lift distribution that neglects three-dimensional effects vs a realistic span-wise trapezoidal lift distribution observed over a finite wing

The lifting-line theory applies the concept of circulation and the Kutta–Joukowski theorem as defined by equation 1. The lifting-line theory states that every spanwise shift in the lift distribution results in the shedding of a trailing vortex [28].

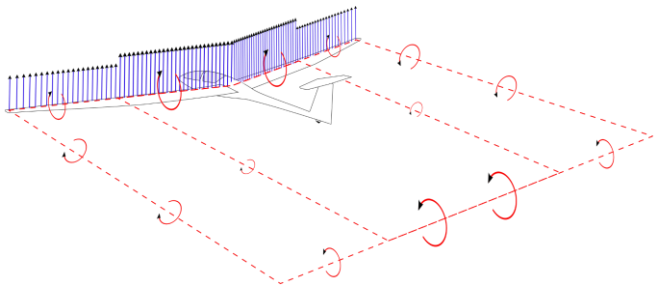

Fig 14: Trailing edge vortices formed by span-wise change in lift distribution

2.5.3 Thin-Airfoil Theory

Hermann Glauert and Max Munk worked together to create the thin airfoil theory. This theory states that the vortices are placed along the mean camber line of an airfoil section to numerically represent the airfoil. The chord line is formed by this arrangement, which creates a vortex sheet. Additionally, the camber line becomes a streamline when the uniform stream is placed on the vortex sheet since the vortex sheet's strength is balanced. This aforementioned flow configuration satisfies the Kutta-condition [3].

2.6 Types of Airfoils and Airfoil Geometry

High lift, general purpose, and high speed are the three categories into which airfoils are separated. Sailplanes and other aircraft with short takeoff and landing distances typically use high-lift airfoil sections. They have well-rounded leading edges, a strong camber, and a high

thickness chord ratio. A lower thickness/chord ratio, less camber, and sharper leading edges are used in general-purpose airfoil sections. High-speed airplanes use high-speed sections. They lack camber, have sharp leading edges, and a very low thickness to chord ratio. [33]

The coordinates of the top and lower surface can be used to describe the geometry of an airfoil. The metrics such as maximum thickness, maximum camber, location of maximum thickness, position of maximum camber, and nose radius are frequently used to summarize it. Given these characteristics, one can design a decent airfoil section. This was accomplished by Eastman Jacobs in the early 1930s to produce the NACA Sections family of airfoils. A broad variety of airfoils were created, mostly through trial and error. The National Advisory Committee for Aeronautics produced the NACA airfoils, which are airfoil shapes for aircraft wings (NACA). The word "NACA" is followed by a string of numerals that describe the shape of the NACA airfoils. The numerical code's parameters can be used to precisely create the airfoil's cross-section and compute its properties. [29], [30]

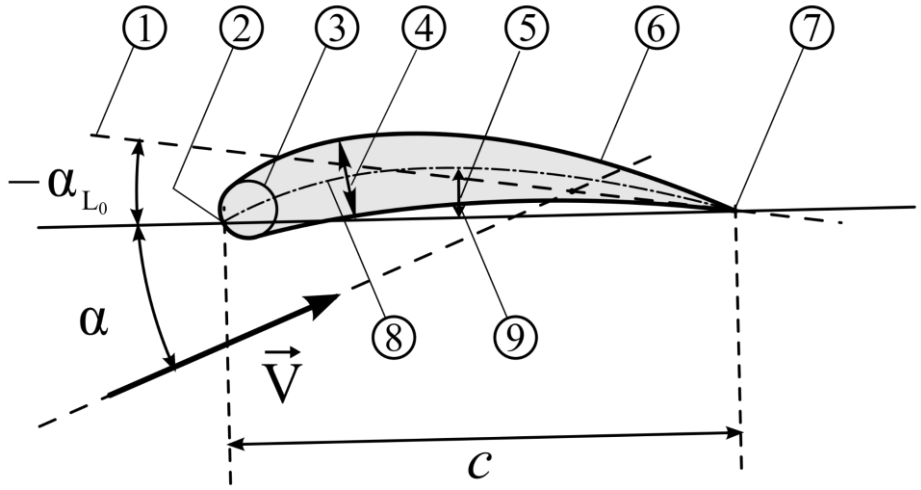

Fig 15: Airfoil geometry: 1: Zero-lift line; 2: Leading edge; 3: Nose circle; 4: Max. thickness; 5: Camber; 6: Upper surface; 7: Trailing edge; 8: Camber mean-line; 9: Lower surface

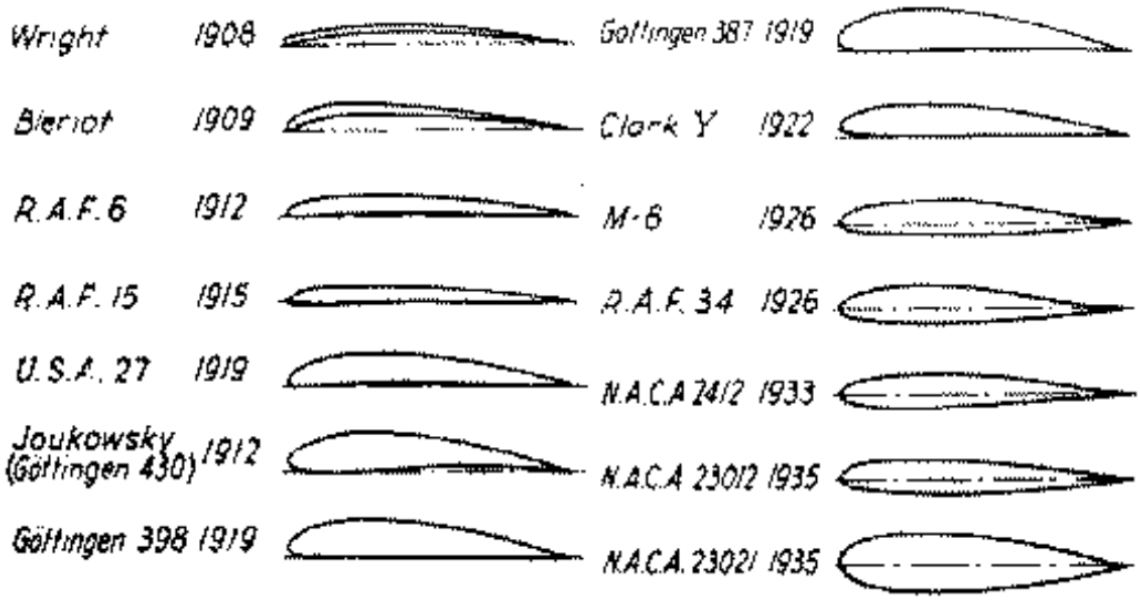

Fig 16: Different airfoil geometries from around early 1900s

The flow conditions and design objectives range from one application to the next, which is one of the reasons why modern airfoils look fairly different from one another and designers have not chosen the optimal airfoil. At very low Reynolds numbers (<10,000 based on chord length) efficient airfoil sections can look rather peculiar as suggested by the sketch of a dragonfly wing. The thin, highly cambered pigeon wing is similar to Lilienthal's designs. The Eppler 193 is a good section for model airplanes. The Lissaman 7769 was designed for human-powered aircraft.

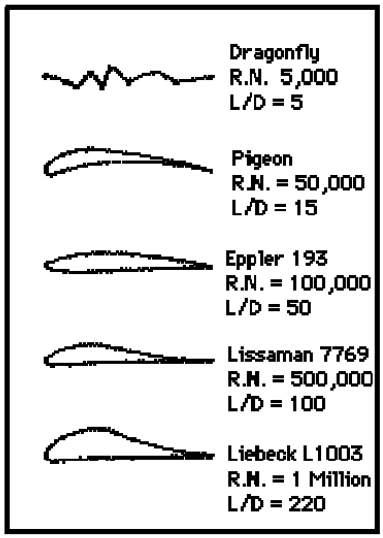

Fig 17: Early airfoil geometries with different range of Reynolds number

Sometimes unusual design restrictions for airfoils can occur, resulting in some unusual shapes. A variable geometry airfoil with a flexible lower surface is one possible alternative with multi-element airfoil being another. The easiest way to study the aerodynamic performance of airfoil sections is to make use of the pressure distribution over the airfoil. Common ways to express this distribution include using the pressure coefficient Cp. [6]

It is important to realize that different airfoils have unique flight properties. There have been countless airfoils studied in wind tunnels and during actual flight, but no single airfoil can meet all of the requirements for a given trip. The shape of each airplane's airfoil is determined by its weight, speed, and intended use. It was discovered many years ago that an airfoil with a concave, or "scooped out," lower surface was the most effective in generating the maximum lift. It was later discovered that this particular airfoil's fixed shape resulted in too much speed loss while providing lift, making it unsuitable for high-speed flight. It's interesting to note, however, when extended from the primary wing structure, leading edge (Kreuger) and trailing edge (Fowler) flaps physically transform the airfoil shape into the traditional concave form, producing significantly more lift during slow flight conditions. [6]

2.7 Concerned Airfoil Profiles

There are probably tens of thousands of airfoil profiles on the internet that one can easily access, but however are not limited to those available only. Designers usually prefer a custom profile based on the requirements and conditions: cruise velocity and flight altitude. A profile can be symmetric, semi symmetric such as Clark Y’s or completely asymmetric, all with varying thickness and aspect ratios. NACA airfoils are the most renowned and widely used airfoil profile with hundreds of subtle variations. Clark Y type geometry and NACA geometry are discussed.

2.7.1 Clark Y Airfoils

Virginius E. Clark created the Clark Y profile in 1922 using the thickness distribution of the German-made Goettingen 398 airfoil. The airfoil is 11.7 percent thick and flat on the lower surface behind 30% of the chord [32]. The flat bottom makes building wings simple and makes it easier to measure angles for propellers. The Clark Y airfoil section has proven to be adequate for many applications; it has mild and generally subtle stall characteristics,

and it provides reasonable overall performance in terms of its lift-to-drag ratio.

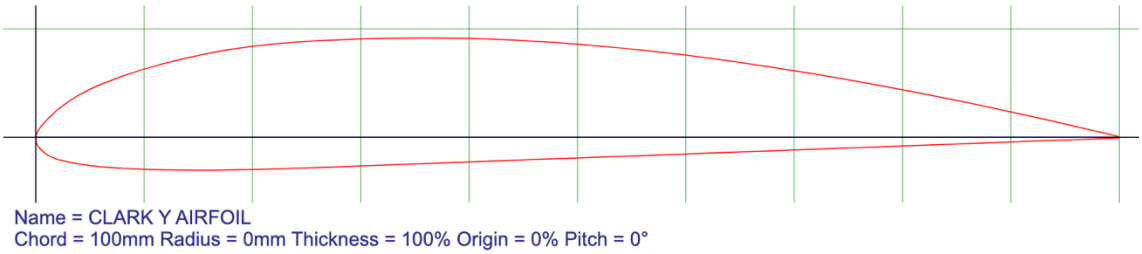

Fig 18: Clark Y airfoil at zero AOA

2.7.2 NACA Airfoils

The NACA (National Advisory Committee for Aeronautics airfoils) created a series of thoroughly tested airfoils in the late 1920s and early 1930s and came up with a four-digit number that indicated each airfoil section's important geometric characteristics. A cross-section of an airfoil was included as a supplement to the numbering system by the time Langley devised this approach in 1929. The full catalog of 78 airfoils then appeared in the NACA's annual report for 1933. The numerical designator ("NACA 2415," for example) specified camber lines, maximum thickness, and unique nose features, allowing engineers to immediately identify the peculiarities of each airfoil shape. [31]

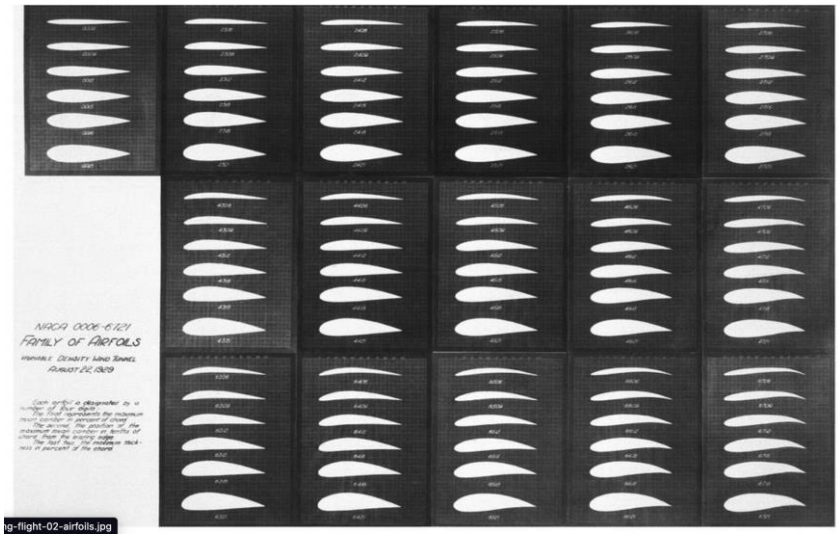

Fig 19: Different NACA airfoil profiles

The four digits that control this NACA Airfoil series, such as NACA 2412, stand for the thickness, maximum camber position, and camber. If an Airfoil number is NACA MPXX, e.g., NACA 2412, M is the maximum camber divided by 100. P is the point of the maximum camber divided by 10 in the case where M=2 and the camber are 0.02 or 2% of the chord. XX is the

thickness divided by 100 in the example where P=4, where the highest camber is at 0.4 or 40% of the chord. The thickness is 0.12 or 12% of the chord in the given case when XX=12. [32]

2.8 Flow Visualization Techniques

Flow analyses are not just simulation constricted. Physics community generally rely on experiments to test, analyze and verify the flow around bodies. Even though simulations make it easier to obtain data without actually putting efforts in experiments, it is recommended that a valid process be set up to validate simulated data. There are different methods to visualize the flow of fluid around bodies such as airfoils. Few of the feasible visualization methods that can be applied to this study are mentioned below.

2.8.1 Smoke Flow Visualization Method

Smoke is a classic visualization method, that involves sending a stream of smoke down the wind tunnel, allowing us to see how airflow interacts with a model in real time. This method can be used with any type of model and in almost any type of wind tunnel. [37]

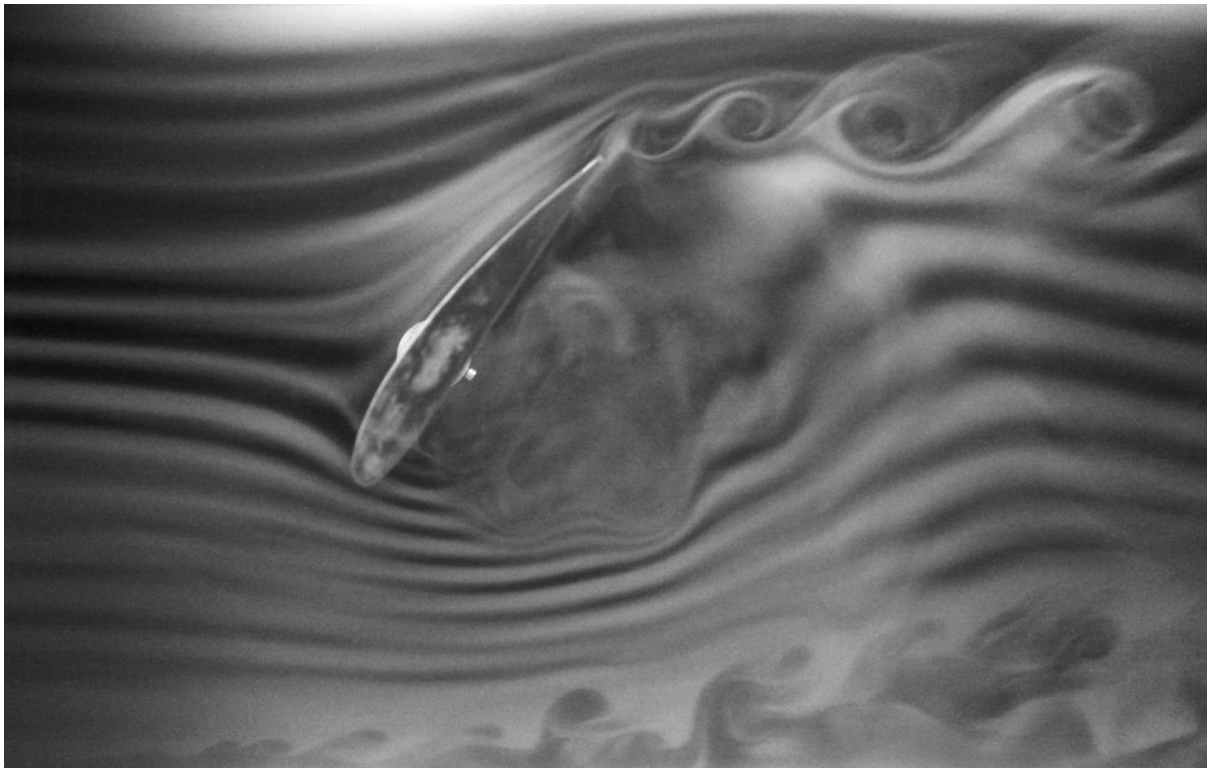

Fig 20: Smoke visualization technique used in an airfoil to visualize laminar flow, turbulent flow, boundary layer separation and vortices around airfoil

2.8.2 Tuft Flow Visualization Method

The Tufts technique uses a filament or string that is attached to the model in one, several, or numerous locations. Tufts resemble grass blades that are blowing in the wind, and numerous tuft installation types include a dye or luminous coating that makes it possible to track movement in ordinary light. It offers details on the surface boundary layer's condition, especially to identify flow separation and reattachment.

Fig 21: Tuft Visualization method to visualize boundary separation

2.8.3 Digital Particle Image Velocimetry

The digital particle image velocimetry method scatters light from particles (oil droplets, smoke particles, etc.) that are seeding into the flow field using pulsed laser sheets. Digital cameras are used to record the dispersed light in order to calculate the positions of each particle on the two-dimensional light sheet. It is feasible to ascertain the particle mobility between the two photos by rapidly pulsing the laser and camera twice. The correlation between the particles in the subsequent photos is calculated for the full flow field using powerful computers, and a two-dimensional map of the flow field velocity is produced.

Chapter 3 Investigation of Airfoil Geometry and Working Methodology

3.1 Multi-Element Wing Geometry

A two-element airfoil system was chosen for the purpose of this research. Among a wide varieties of airfoil profiles and geometries, Clark y was chosen as a subject of study for its' geometric simplicity. Clark y excludes complex curves at lower planform area and instead replaces it with a simpler plane. This makes the creation of airfoil geometry less tedious in comparison with other profiles such as NACA. No geometry optimizations were done on to the airfoil, hence the study focuses on behavior of different arrangements of clark y airfoils.

The basis of comparison or geometry selection finalization does not end with the simplicity of the profile, instead, Clark y's are often used in low flight applications such as commercial airlines. Clark Y's do not have multiple varieties like NACA, which is one of the leading reasons for choosing them.

An airfoil geometry plays an important role in determining the total lift as well as drag forces associated with the system, which ultimately depends on the application type of the wing. But since this research is based more on the behavioral study of multi-element wings and less on its applications, geometry type does not create a significant difference overall.

Clark Y profile used in this study has following properties

Chord length of bigger element: 150mm at 100% size

Chord length of smaller element: 60mm at 40% size

Max thickness: 8.81% at 34.26% chord length

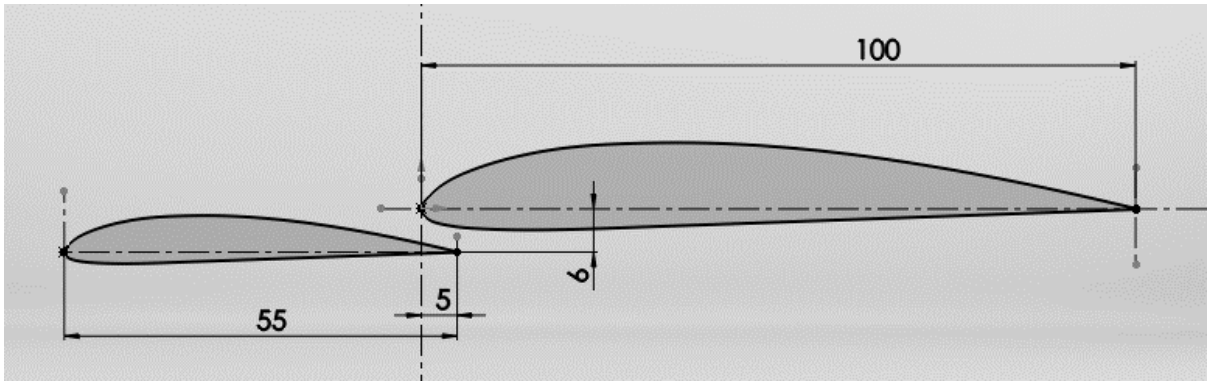

Fig 22: Two element Clark-Y airfoil with a gap of 5mm and overlap of 6mm constructed using Solidworks 2D. Dimensions are explained in section 2.3

3.2 Double-Element Profile Orientations

3.2.1 Profile 1: With upper flap

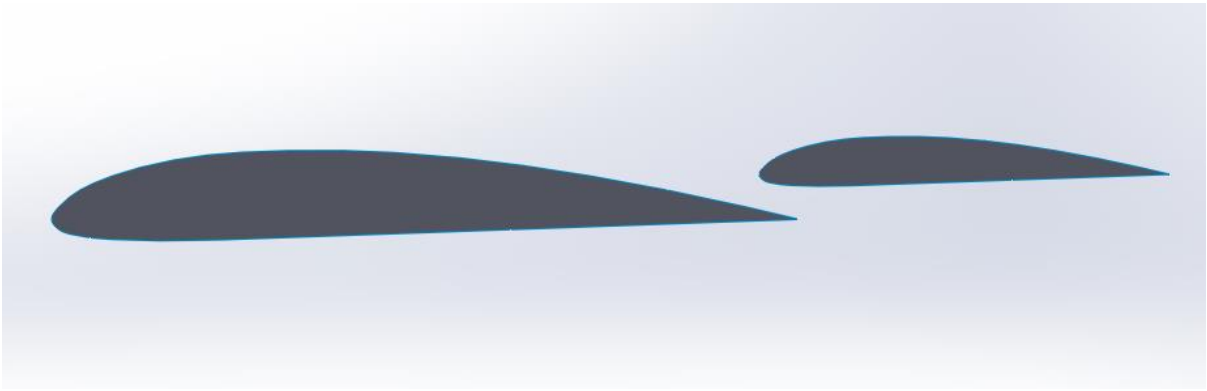

Fig 23: Double element orientation with flap above the trailing edge of main element

3.2.2 Profile 2: With lower flap

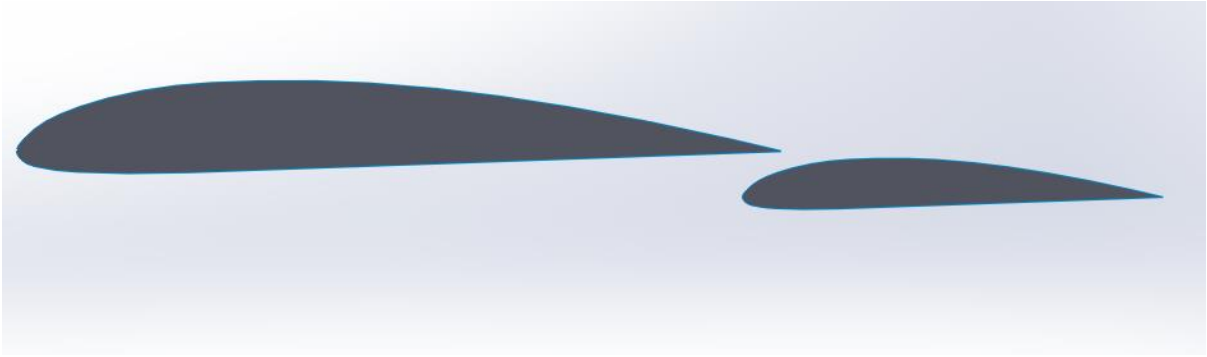

Fig 24: Double element orientation with flap below the trailing edge of main element

3.2.3 Profile 3: With upper slat

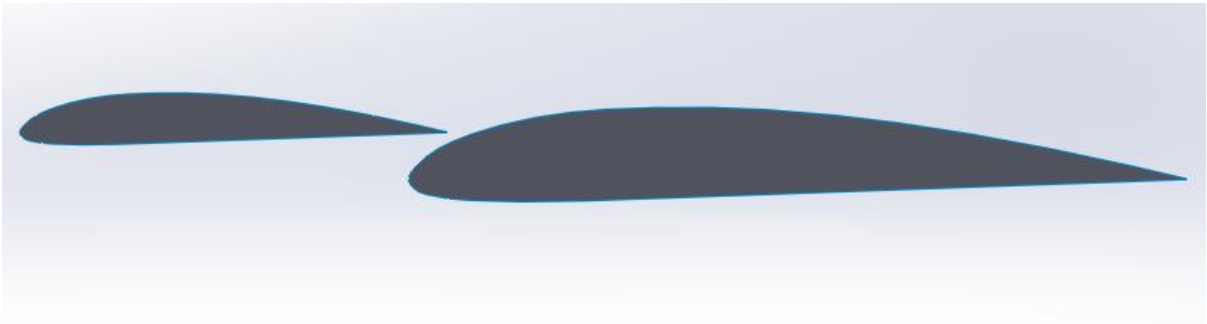

Fig 25: Double element orientation with slat above the leading edge of main element

3.2.4 Profile 4: With lower slat

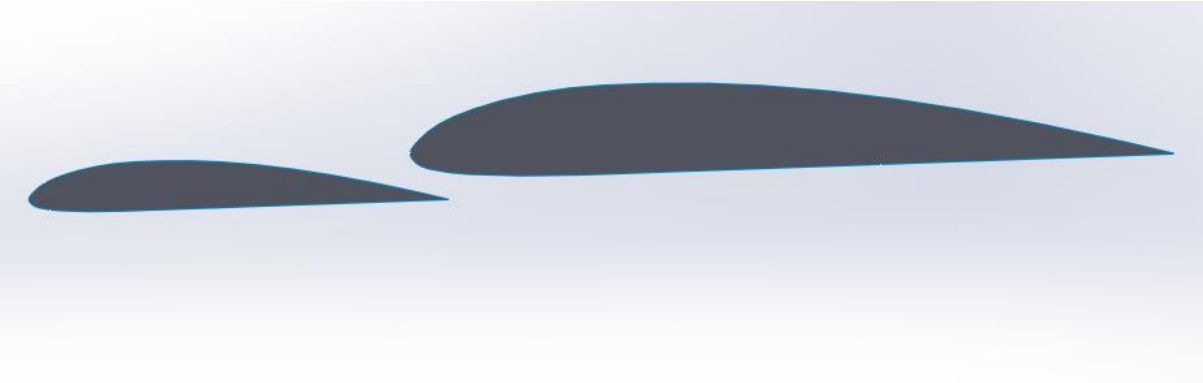

Fig 26: Double element orientation with slat below the leading edge of main element

3.3 Methodology Blueprint

Figure 26 showcases a 2D sketch of two-element airfoils created using a modeling software. The geometry is then converted to a 2D surface using the feature from same software and then is transferred to Ansys for further computational simulation. However, several geometry profiles will be created with differences such as orientation and angle of attack of the elements. For example, in a two-element airfoil, placement of the small element can be in front or behind the main airfoil. This means, the gap and overlap can have a certain value as of simplicity but the values can still be attained with positive and negative magnitude, making different orientations even with just two elements. This is shown in figure 22.

Flow simulations are performed on all such orientations and the arrangement with maximum benefits (such as high lift or low drag) will be put forward for further simulations on varying angle of attacks. Figure 23-25 shows images with zero degrees of angle of attack.

Another approach is also proposed in which a Clark Y profile is geometrically broken into multiple elements based on the location of air flow separation. With such broken geometries, higher performance (Cl/Cd) of the wing is expected. The geometry can be broken into multiple elements: 2, 3 and more, but since the process is iterative and tedious, the study is focused only on the limited number of elements.

The airfoil geometry shown in the figure 26 was built in Solidworks using the co-ordinates extracted from the airfoil database mentioned in reference 32. The co-ordinates were then converted into curved sketches in 2D.

3.4 Dimensional Analysis and Modeling

Maintaining dimensional homogeneity and equation applicability is the major goal of performing dimensional analysis between experiment prototypes and models. In order to achieve this, the equation's parameters are non-dimensionalized, resulting in a separate set of dimensionless parameters that are independent to model/prototype dimensions and/or flight conditions. What it does is make the overall calculations and analyses easier, first by reducing the number of parameters in itself, and second, by reducing the number of experiments to be performed. It also obtains scaling laws so that prototype performance can be predicted from model performance. To put it simply, dimensional analysis is the comparison of similarities between a model and a prototype to preserve experimental consistency by forcefully getting rid of otherwise associated dimensions. [34]

Typically, a characteristic length (L), a characteristic velocity (v), and a reference pressure difference (P_0-P_∞) are the scaling parameters in a fluid flow problem. Density, viscosity, and gravitational acceleration are a few other variables and fluid properties that enter the equation. There are three necessary conditions for a complete similarity between a model and a prototype.

- Geometric similarity: Similarity in the shapes
- Kinematic similarity: Similarity in flow velocities
- Dynamic similarity: Similarity in forces involved

All three similarities must exist for complete equivalence to be ensured.

3.5 Dimensional Irrelevance

Consider a multi-element wing is being designed for an airplane and its total lift is to be predicted. The chord length is Lc for the biggest element and reduces on a percentage basis for the rest of the elements. The prototype of the wing is to be tested at $v_{prototype}$. A 1:x scale model is built to be tested in a pressurized wind tunnel that can be pressurized to a maximum pressure P. Here a final functional relationship is required where dimensional parameters become irrelevant.

This can be done by making use of Method of Repeating Variables [32]. Important parameters that define the characteristics of the performance of the wing are listed as below.

- Chord length (L_c)
- Max camber height (c), overlap, gap

- Angle of attack
- Model scale (1:x)
- Free stream velocity (v)
- Density of undisturbed air
- Planform area (A)

Since both model and prototype are examined under same angle of attack, it is constant for both and can be neglected. Configuration geometry such as overlap, gap and camber height are inclusive in scale ratio. Hence, remaining parameters are

- Scale ratio (1:x)
- Free stream velocity (v)
- Density of undisturbed air (ρ)
- Viscosity of air (μ)
- Planform area (A)

The primary dimensions (j) of each parameter (n) are

$Lc = \{L\}$, $v = \{LT^{-1}\}$, $\rho = \{ML^{-3}\}$, $\mu = \{ML^{-1}T^{-1}\}$

Since there are three primary dimensions involved, according to Buckingham's Pi theorem, expected number of independent parameters (π) is given by

$K = n-j = 4-3 = 1$

Dynamic viscosity can be combined with density to form kinematic viscosity and reduce n and j each by 1.

$\vartheta = \{L^2T^{-1}\}$

$n= 3$ and $j = 2$

$k = 1$

The chosen repeating parameters are: i) Velocity (v) for its simplicity and all dimensional inclusivity and ii) Kinematic viscosity (ϑ) dimensional inclusivity.

The dependent non-dimensional parameter is given by

$\pi = Lc.v^a.\vartheta^b$

Dimensionally, $[L].[LT^{-1}]^a.[L^2T^{-1}]^b = 1$

$[L^{1+a+2b}].[T^{-a-b}] = 1$

$a= 1, b= -1$

Therefore, $\pi = L_c.v^1.\vartheta^{-1}$

$$\pi = \frac{L_c v}{\vartheta}$$

which is also the analogy to Reynold's number.

Hence, by embracing non-dimensionality of Reynold's number, systems are governed by constant values and parameters such as free stream velocity, kinematic viscosity and characteristic length become irrelevant to discuss because all these parameters have been included into the Reynold's number. Other dimensionless parameters widely used in fluid mechanics are coefficient of lift, coefficient of drag and et. al. By using these constant values, independent parameters such as velocity or pressure or density are eliminated from the system.

Reynold's number is given by

$$Re_m = \frac{\rho_m \times v_{m \times} L_m}{\mu_m}$$

for model, and

$$Re_p = \frac{\rho_p \times v_p \times L_p}{\mu_p}$$

for prototype, where

ρ = fluid density, v = flow velocity, L = characteristic length and μ = dynamic viscosity of fluid

Similarity is attained as long as the corresponding independent dimensionless parameters are both set equal to each other. This holds true despite the fact that the working fluids have entirely different properties such as density and viscosity. Further relationship between model and prototype is given by

$$v_m = v_p \left(\frac{\mu_m}{\mu_p}\right)\left(\frac{\rho_m}{\rho_p}\right)\left(\frac{L_m}{L_p}\right)$$ **----------Equation 9**

And, lift generated on the wing can be numerically calculated using the pressure difference above and below the wing. Or, lift force can be replaced with coefficient of lift to maintain homogeneity and comparability among other wings or orientation.

3.6 Output Visualization Methodology

3.6.1 C_p vs x/c Graph

Generally, Cp vs x/c is plotted to visualize airfoil pressure distribution over the camber length. Generally, x/c is the x-location normalized over chord length c. At the leading edge, x/c is 0,

whereas at the trailing edge, it is 1. Cp is displayed "upside-down" on the plot, with negative values (suction) positioned higher. (This is done to make sure that the upper curve and the upper surface of a typical lifting airfoil correspond.) At the stagnation point close to the leading edge, the Cp begins at a value of roughly 1.0. On both the top and lower surfaces, the pressure falls quickly before recovering to a modest positive value of Cp close to the trailing edge.

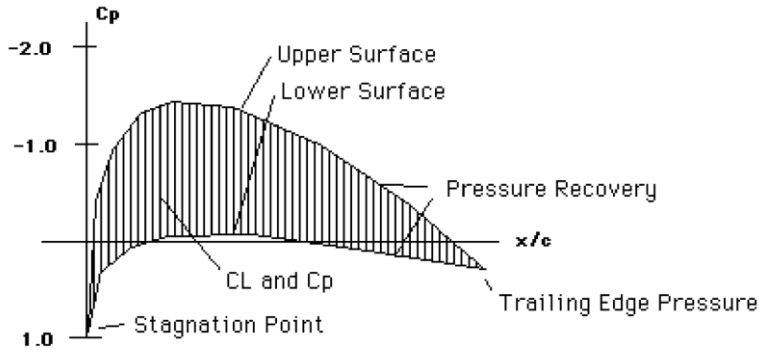

Fig 20: Cp vs x/c to visualize pressure distribution over camber length

- Upper Surface: The pressure on the upper side of the curve is lower and hence creates the suction effect
- Lower Surface: The lower surface has a positive pressure, but in certain design conditions the role of the lower surface is actually pulling the wing downward. In this case, some suction (negative Cp- downward force on lower surface) is present near the mid-chord.
- Pressure Recovery Region: The zone of pressure distribution over span length is called pressure recovery region
- Trailing Edge Pressure: The pressure at the trailing edge of an airfoil or wing is important because it plays a key role in determining the lift and drag forces acting on the wing. The pressure distribution over the surface of an airfoil is affected by the angle of attack, the shape of the airfoil, and the speed of the air flow. The pressure difference between the upper and lower surfaces of the wing generates lift, while the pressure difference between the front and back of the wing generates drag. The pressure at the trailing edge can also influence the stability and control of an aircraft, as changes in the trailing edge pressure can affect the way the wing responds to changes in angle of attack or speed.

- C_L and C_P: The coefficient of lift is a measure of how effectively an object generates lift, or the force that allows it to rise into the air. It is typically defined as the lift force generated by an object divided by the dynamic pressure of the fluid (such as air) it is moving through and the surface area of the object. A higher coefficient of lift indicates a more efficient lift force.

The coefficient of drag is a measure of how much resistance an object experiences as it moves through a fluid. It is typically defined as the drag force experienced by an object divided by the dynamic pressure of the fluid and the surface area of the object. A higher coefficient of drag indicates a greater resistance to motion. The pressure distribution on an airfoil plays a critical role in its performance. The pressure distribution determines the lift and drag forces acting on the airfoil, which in turn affect its ability to fly and maneuver. Following figure shows how pressure distribution is related to airfoil performance.

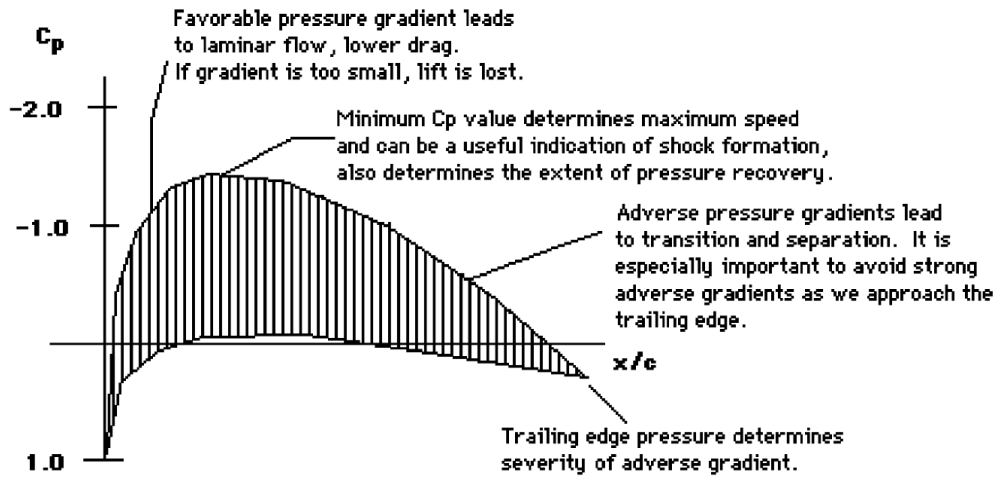

Fig 21: Relation between pressure distribution and airfoil performance

- Pressure Coefficient (C_p)

Pressure distribution over a body surface can be specified through the non-dimensional parameter, i.e., pressure coefficient.

$$C_p = \frac{P - P_\infty}{\rho v^2/2}$$ ----------**Equation 10**

Pressure coefficients around similar bodies of different sizes in flows of different velocities will be same if the Reynold's numbers of these flows are same. However, the corresponding pressures and velocities can be different. To measure pressure coefficients in experiments, static pressures should be measured initially, one being on the surface (P_o) and the other being in the area of undisturbed flow (P_∞), ideally far upstream of the body.

In order to calculate the velocity of the flow, it is convenient to measure velocity at the stagnation point where the velocity becomes zero ideally, after impact. Hence, the pressure at stagnation point is given by

$$P_o = P_\infty + \frac{\rho v^2}{2}$$

And, $$\frac{\rho v^2}{2} = P_o - P_\infty$$

Which is simply a manometer reading at α = 0. Then to obtain the pressure coefficient at any α, it is sufficient to divide the corresponding manometer reading by the stagnation point reading, i.e.,

$$C_p = \frac{P(\alpha) - P_\infty}{P_o - P_\infty}$$ ----------**Equation 11**

3.6.2 C_L vs Re Plot

A graph between Coefficient of lift and Reynolds number is plotted to envision lift coefficient of the wing varying over different Reynolds number. The values for coefficient of lift and Reynold's number are obtained from wind tunnel tests, where C_L is calculated as given by equation 2. The planform area, density and velocity of air are constant for the setup and can be easily measured, whereas the lift force can be slightly tricky to calculate. But if a weighing machine (based on grams) could be placed beneath the airfoil stand, difference in mass before and after the air flow can be measured and multiplied by g to obtain the lift force. With all the given information, C_L can be calculated using excel or MATLAB for all given points along the airfoil surface and a functional form of the relation can be derived through regression. Meanwhile, Reynold's number can be calculated with known properties of air (kinematic viscosity), Characteristic length (diameter of wind tunnel) and freestream velocity of air.

Chapter 4 Computational Setup, Results and Discussions

4.1 Simulation Setup

4.1.1 About ANSYS

A robust computational fluid dynamics (CFD) tool called ANSYS Fluent is frequently employed in engineering and academic studies. One of its primary uses is flow visualization, which enables users to comprehend the intricate behaviors of fluids in a variety of situations. Users may simulate fluid flows in 2D and 3D environments with ANSYS Fluent, view the findings, and evaluate them to improve designs. Such simulations are usually performed to avoid expenses or tediousness of laboratory-based experiments. The software can quickly and easily study and interpret flow behavior through a variety of visualization options included in the program, such as contour plots, vector plots, and animations. ANSYS is often a preference among students for its versatility and UI simplicity when dealing with computational fluid dynamics. The recreation studies made under this report were also based on ANSYS.

4.1.2 Standardized Simulation Parameters

Following simulation standards were fixed on different parameters and were followed by the authors for simulation uniformity.

- Import type: IGES format exported by Solidworks
- Analysis type: 2D
- Reference frame: Lagrangian
- Type of co-ordinate system: Cartesian
- Solver preference: Fluent
- Mesh smoothing: Medium
- Mesh growth rate: 1.2 times
- Mesh type: Number of divisions
- Mesh divisions: 500
- Active bias growth rate: 1.2
- Mesh refinement: 3 times

4.1.3 Turbulence Modeling Methods

There are multiple approaches to the modeling of turbulence in CFD; they are mainly characterized by the mesh resolution of the problem, which in return defines the computational power needed for a simulation.

- Direct Numerical Simulation (DNS)

DNS is a high-resolution mesh that can resolve the turbulent flow's smallest spatial and temporal scales is called a Direct Numerical Simulation (DNS). The structure of the turbulence in DNS is totally represented. However, the computational cost associated with DNS is extremely high. Thus, DNS is limited to small-scale problems with low Reynolds numbers.

- Reynold's Average Numerical Simulation (RANS)

The RANS equations are derived from the Navier-Stokes equations, which are a set of equations that describe the motion of fluids. The Navier-Stokes equations are a set of differential equations that describe the conservation of mass, momentum, and energy in a fluid. However, these equations are very complex and difficult to solve, especially for complex flow systems. To simplify the Navier-Stokes equations, the concept of a Reynolds average was introduced which allows the Navier-Stokes equations to be rewritten in a form that is more suitable for numerical solution. In this form, the equations are known as the Reynolds Average Navier-Stokes (RANS) equations. The RANS equations are a collection of partial differential equations that explain how a fluid behaves in terms of its mean velocity, mean pressure, and mean temperature.

- Large Eddy Simulation (LES)

In a Large Eddy Simulation (LES) turbulence model, the smallest scales of turbulence are spatially filtered out to be modeled. While the largest, most energy-containing scales are resolved directly by the mesh. This approach allows for having a coarser mesh resolution than in DNS and hence making this method to be more universal and applicable to various fluid flow problems. This method however, has not been used within this study.

- Detached Eddy Simulation (DES)

Detached Eddy Simulation turbulence models combine the methodology from both RANS and LES models. In the region near the wall where the turbulence length scales are smaller than the maximum grid size, the DES model assigns a RANS model to that region. Consequently, in regions where the turbulent length scales are larger than the maximum grid size the DES model

assigns an LES model to that region. This approach allows for reducing the computational cost associated with the simulation since the grid resolution does not need to be as demanding as a pure LES simulation [38]. DES has not been used in this study.

4.1.4 Solution Algorithms

- SIMPLE (Semi-Implicit Method for Pressure Linked Equations)

Simple algorithms are numerical techniques used in computational fluid dynamics (CFD) to attempt to solve the Navier-Stokes equations, which describe the behavior of fluids like air and water. With an emphasis on reducing the time and resources needed to run simulations, these algorithms are created to be reasonably simple to implement and computationally efficient. The fluid domain is discretized into a grid of cells in simple algorithms using the finite difference or finite volume method, which approximates the equations regulating fluid behavior at each cell. Additionally, they might make use of streamlined representations of turbulence or other complex fluid behavior, such as the k-epsilon model or the Reynolds-averaged Navier-Stokes (RANS) equations. [38]

- SIMPLEC (SIMPLE Consistent)

Same as SIMPLE algorithm except momentum equations are manipulated so that the SIMPLEC velocity correction equations omit terms that are less significant than those in SIMPLE. SIMPLEC has not been used to initialize the solutions within this study.

- PISO (Pressure Implicit with Splitting of Operators)

The PISO algorithm is a widely used method for solving the Navier-Stokes equations. It is known for its versatility in handling a variety of fluid flows, including those with severe shocks and vortices. Its full name is Pressure-Implicit with Splitting of Operators. On a mathematical level, the PISO algorithm operates by implicitly solving the pressure equation while iteratively solving the momentum and continuity equations. It can handle non-orthogonal grids and unstructured meshes and employs a predictor-corrector methodology to guarantee that the solutions are consistent and stable.

4.2 Simulation Results Approach 1: Unbroken Geometry

4.2.1 Single-Element Profile

Unbroken profiles for multi-element wings are simple airfoil geometries that are stacked along one another. Such unbroken geometries as shown in section 3.1 are devoid of complex assemblies and consists of entire airfoil (Clark Y as proposed in this study) oriented one after another. The analogy for stacked orientation is quite intuitive in nature does not require much thoughts to grasp the ideas. Every element in this analogy works individually creating a portion of total lift and a portion of total drag. Addition of elements each add lift and drag, but each front element affects the potential performance of rear elements by disrupting the air flow around them. Hence the motive of computational analysis of this research has been to qualitatively look at such performances and quantify them as necessary.

Simulations have been performed on two element airfoils with four different orientations. Performance of a Clark Y is also imitated using ANSY Fluent thus visualizing its pressure and velocity fields graphically as shown.

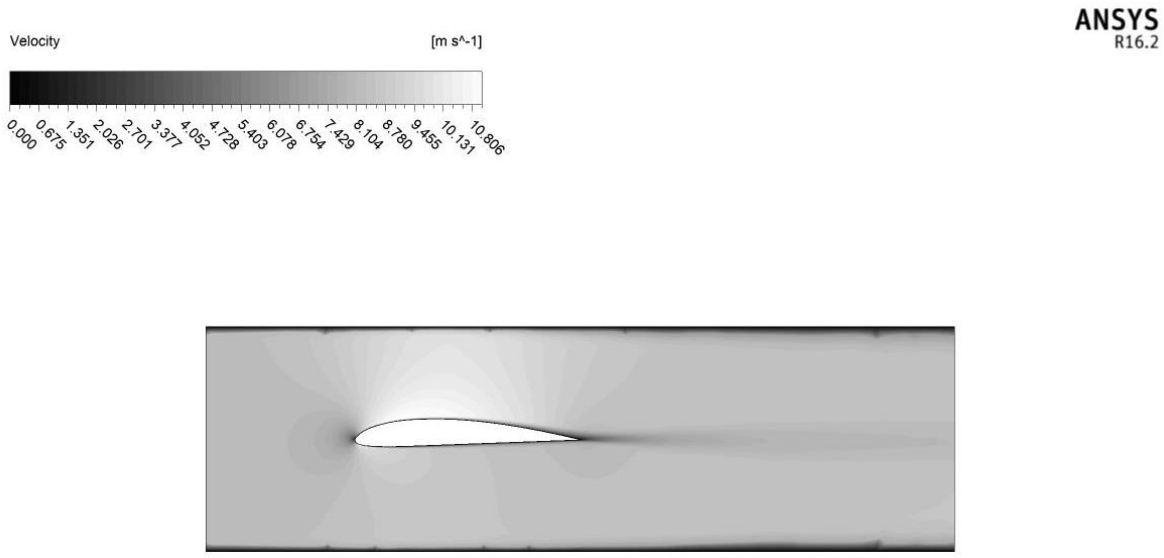

Fig 27: Velocity distribution contour for Clark Y airfoil

At an orientation of 0 degrees of attack angle, the Clark Y submits a swift raise in velocity at both the upper and lower surfaces, with comparatively higher magnitude at upper surface. Raised velocity at the lower surface is unwanted as it reduces the static pressure around the flow zone. Reduced static pressure at lower regions comply to poor lift performances for the Clark Y at 0 degrees. Increased angles of attacks might resemble different circumstances, but however, a single element is not at much highlights within this research domain. Figure 28

displays airflow separation at the inlet flow velocity of 8 m/s starting at around maximum thickness. Air flow separation as discussed in chapter 1 creates pressure drag on the wing.

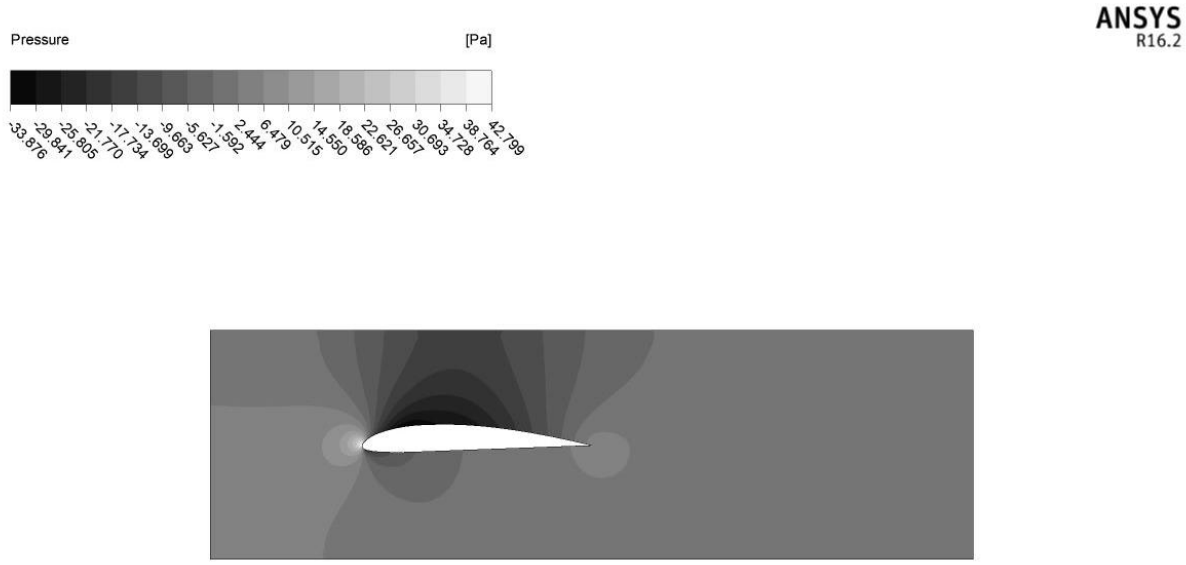

Fig 28: Pressure distribution contour for Clark Y airfoil

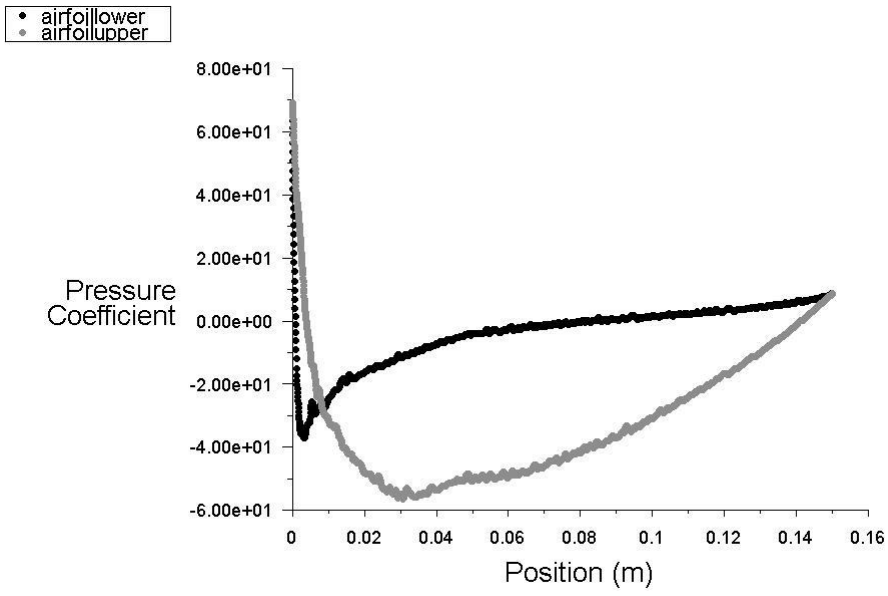

Fig 29: Graph representing Pressure coefficient as a function of distance

Pressure coefficient is plotted against position (in meters), and shows poor performance of the Clark Y airfoil at leading edge with unwanted lower pressure values on lower surface. This could be avoided and improved by increasing AOA of the profile. The profile also shows a tendency to separate the airfoil at x=50mm from leading edge. This could be a reference to break down airfoil geometry into another element in further iterations.

4.2.2 Double-Element Profile 1 at 0 degrees AOA

Pressure field for double element airfoil profile with a 60% smaller element as a slat positioned in front is as shown. This orientation is named as Profile 1 to omit any emerging confusions and the slat is positioned 6mm below the main body.

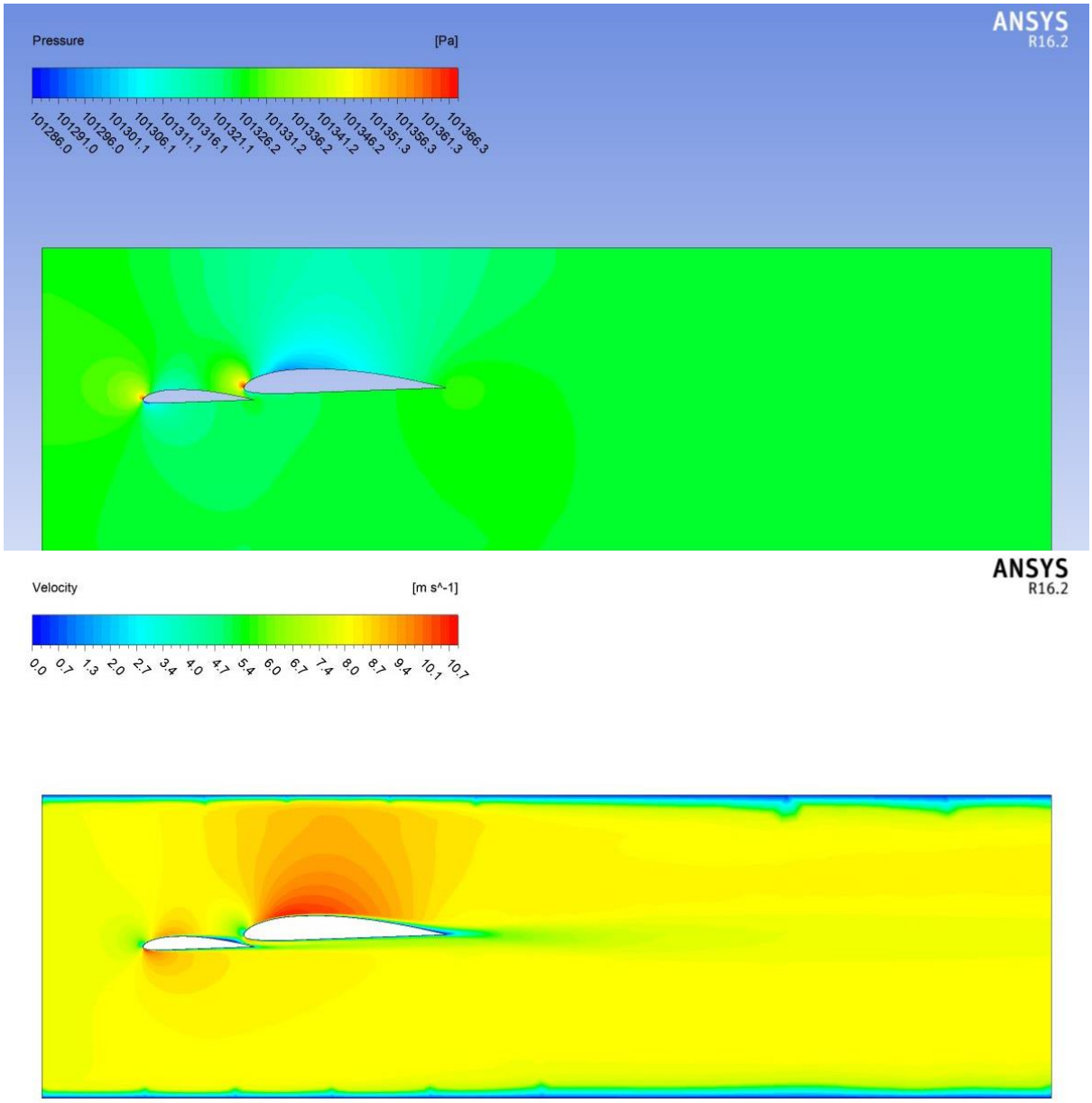

Fig 30: Pressure and Velocity distribution contour for profile 1

Simulations show poor pressure distribution along the slat, with minimal difference above and below the slat surface, whereas the pressure at upper region seems favorable for the main element at 101,301 Pa minimum considering ambient pressure of 101,330 Pa.

4.2.3 Double Element Profile 2 at 0 degrees AOA

Pressure field and velocity contours for double element airfoil profile with a 60% smaller element as a slat positioned in front is as shown. This orientation is named as Profile 2 and the slat is positioned 6mm above the main body.

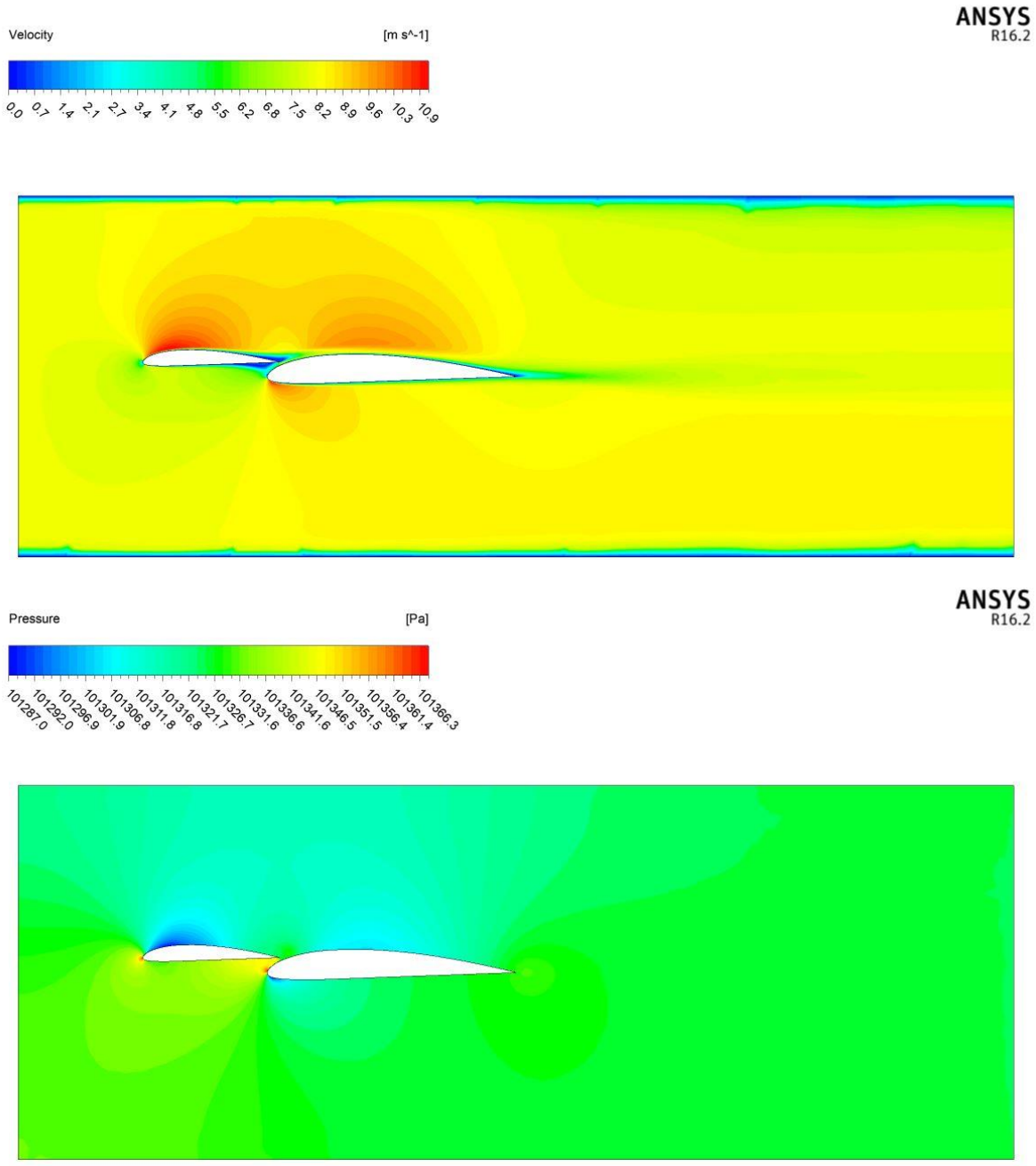

Fig 31: Pressure and Velocity distribution contour for profile 2

With slat positioned above and in front the main element, Profile 2 seems to display a better pressure difference above and below the airfoils. The effect of slat is positive for the overall orientation as the distribution is spread along the entire surface.

4.2.4 Double Element Profile 3 at 0 degrees AOA

Pressure field and velocity contours for double element airfoil profile with a 60% smaller element as a flap positioned behind is as shown. This orientation is named as Profile 3 and the flap is positioned 6mm above the main body.

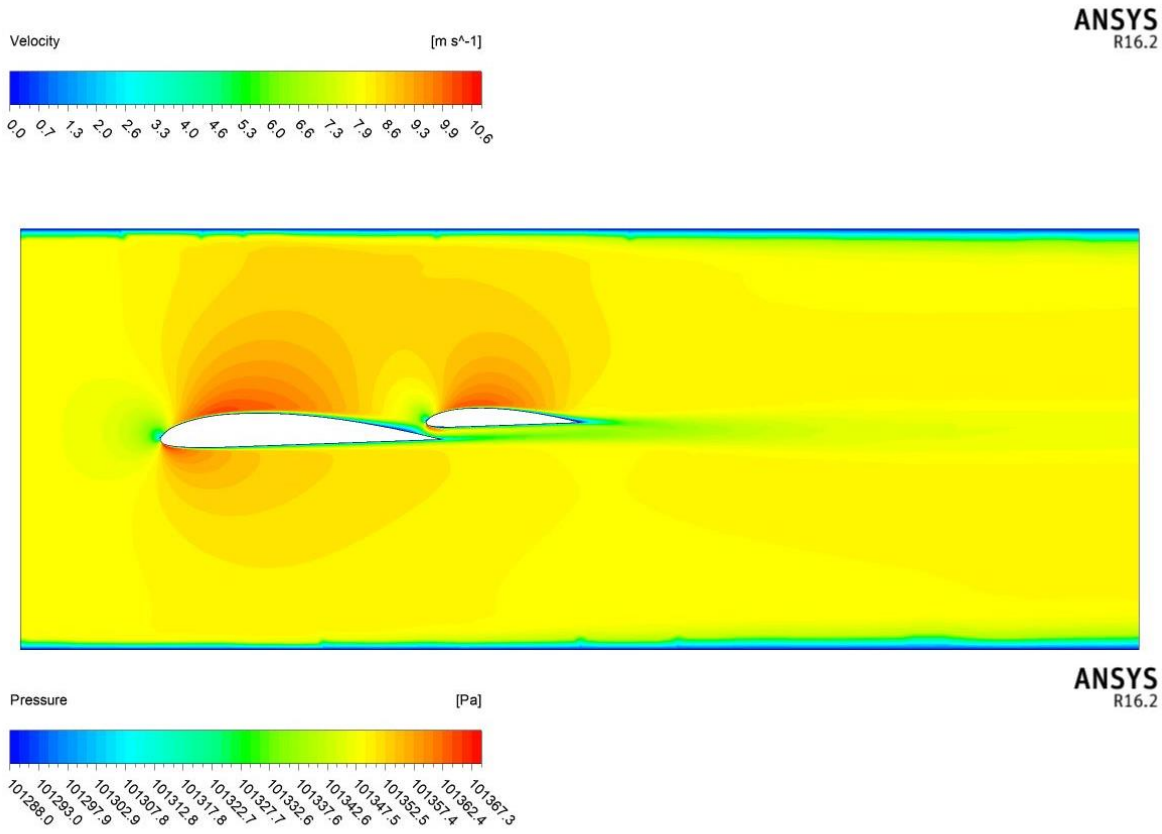

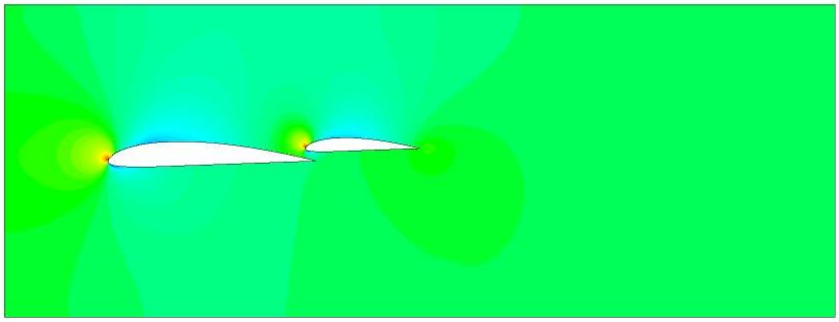

Fig 32: Pressure and Velocity distribution contour for profile 3

Similar to profile 1, this specific orientation shows poor distribution of low-pressure zone between the surfaces. Also, the magnitude of pressure difference does not create any significance at all.

4.2.5 Double Element Profile 4 at 0 degrees AOA

Pressure field and velocity contours for double element airfoil profile with a 60% smaller element as a flap positioned behind is as shown. This orientation is named as Profile 3 and the flap is positioned 6mm below the main body.

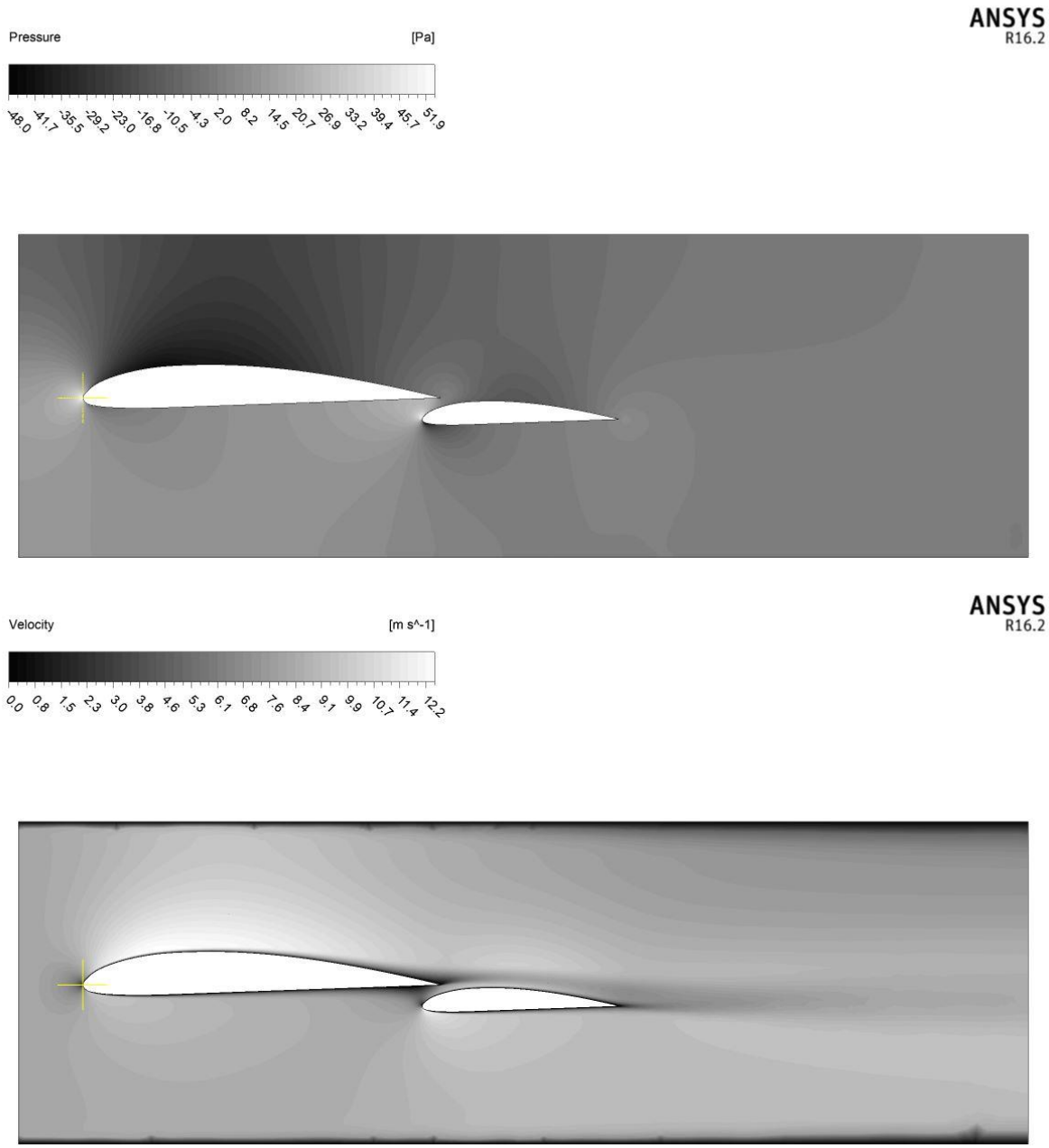

Fig 33: Pressure and Velocity distribution contour for profile 4 in grayscale

Simulation results on profile 3 shows the best results by far among all orientations made at 0 degrees of AOA. The pressure difference between upper and lower surface is distinct with smooth distribution over all. Better results could be obtained if AOA for the flap is increased to certain degrees. Air flow directed by the main element is stagnated at the tip of the flap thus

reducing potential performance. With increase in AOA, this should be eliminated and the pressure distribution should be smoother. Further study on increased AOA is discussed on upcoming sections.

4.2.6 Double Element Profile 4 at 5 degrees Flap AOA

Profile 4 promised better performance for lift as discussed in section 4.2.5. But the analysis was done for 0 degrees AOA, which is often insufficient and insignificant in terms of applications of airfoils. Airplane wings often cruise at AOA greater than 0 whenever maximum lift is required, which makes it necessary for this study to approach the multi-element wings at AOA higher than 0 degrees. Figure below shows pressure and velocity distribution of double elements placed at an attack angle of 5 degrees and at an inlet velocity of 8m/s. Pressure field given as input is relative in nature, and hence, a minimum of (ambient pressure) 101,330 Pa - 56.272 Pa pressure zone is distributed along upper surface of the profile and a maximum of 101,330 Pa + 23 Pa is phased out along lower surface.

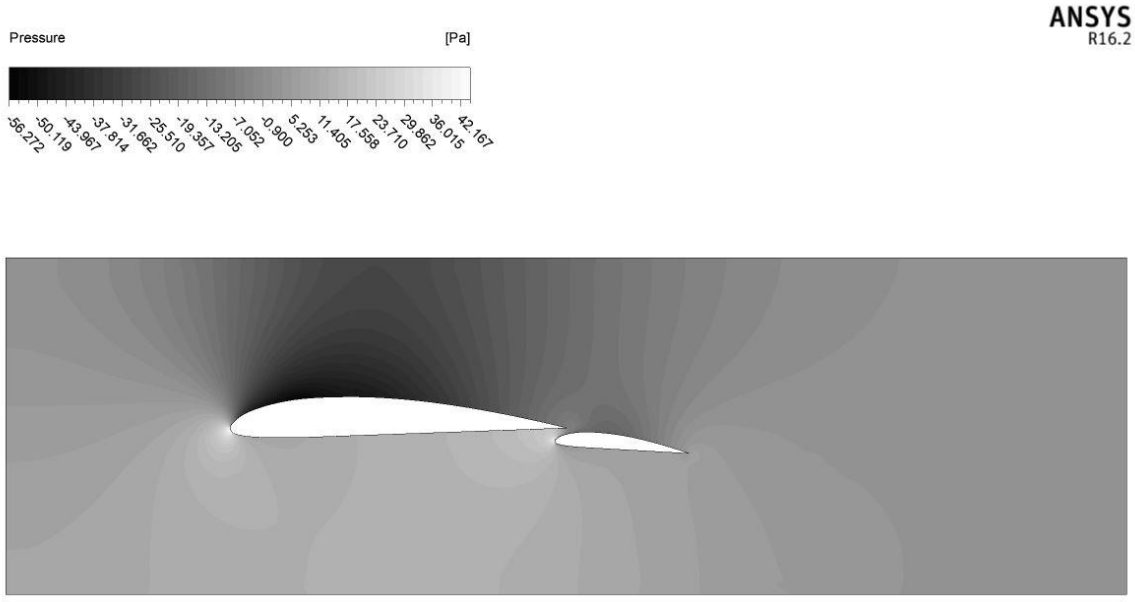

When looked at, the velocity contours in figure 34 illustrates sudden plummeting of velocity at around 80% chord length, which is caused as a result of air flow separation. Even at air flow velocities as low as 8 m/s, Clark Y yields air flow separation, which in return amplifies the lift of the flap by reducing pressure at that zone. However, even though drag effects are not discussed, increase in lift and increase in overall drag are causality for the airfoil system and severe air flow separation can even stall the wings.

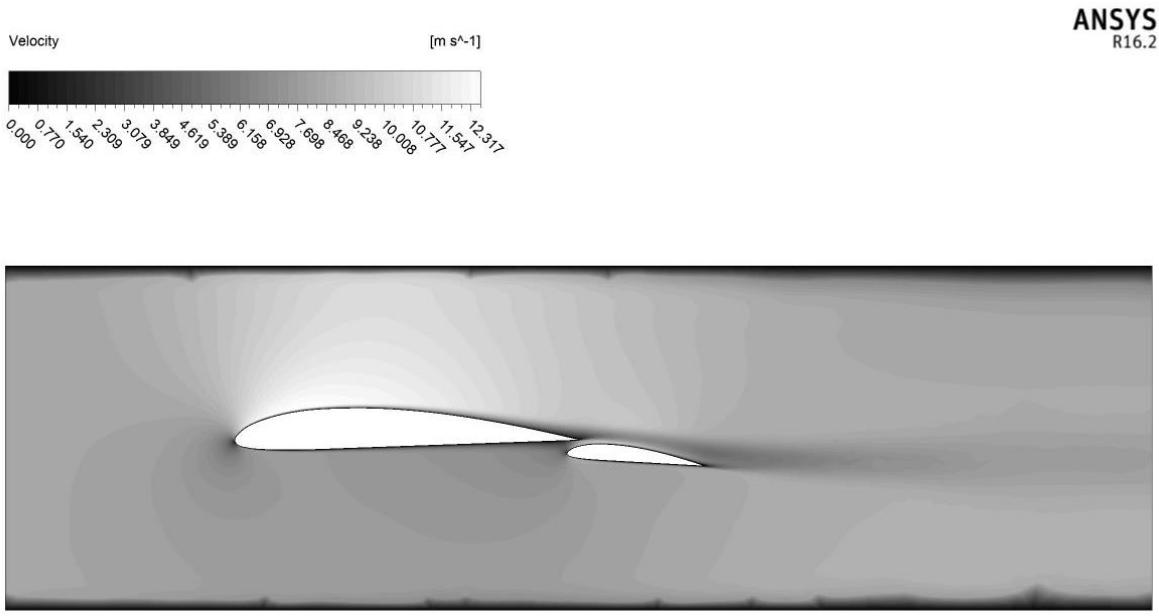

Fig 34: Pressure and Velocity distribution contour for profile 4 at 5 degrees of flap AOA

4.2.7 Double Element Profile 4 at 10 degrees Flap AOA

Simulation contours of pressure distribution around the surfaces and velocity contours for both the double element profiles with 5 degrees and 10 degrees look qualitatively similar. There does not seem to be any significant differences especially in the main element. But for the 60% smaller flap, 10 degrees of AOA has delivered slightly higher upstream velocity of about 12 m/s in compared to the 5 degrees AOA with 9 m/s.

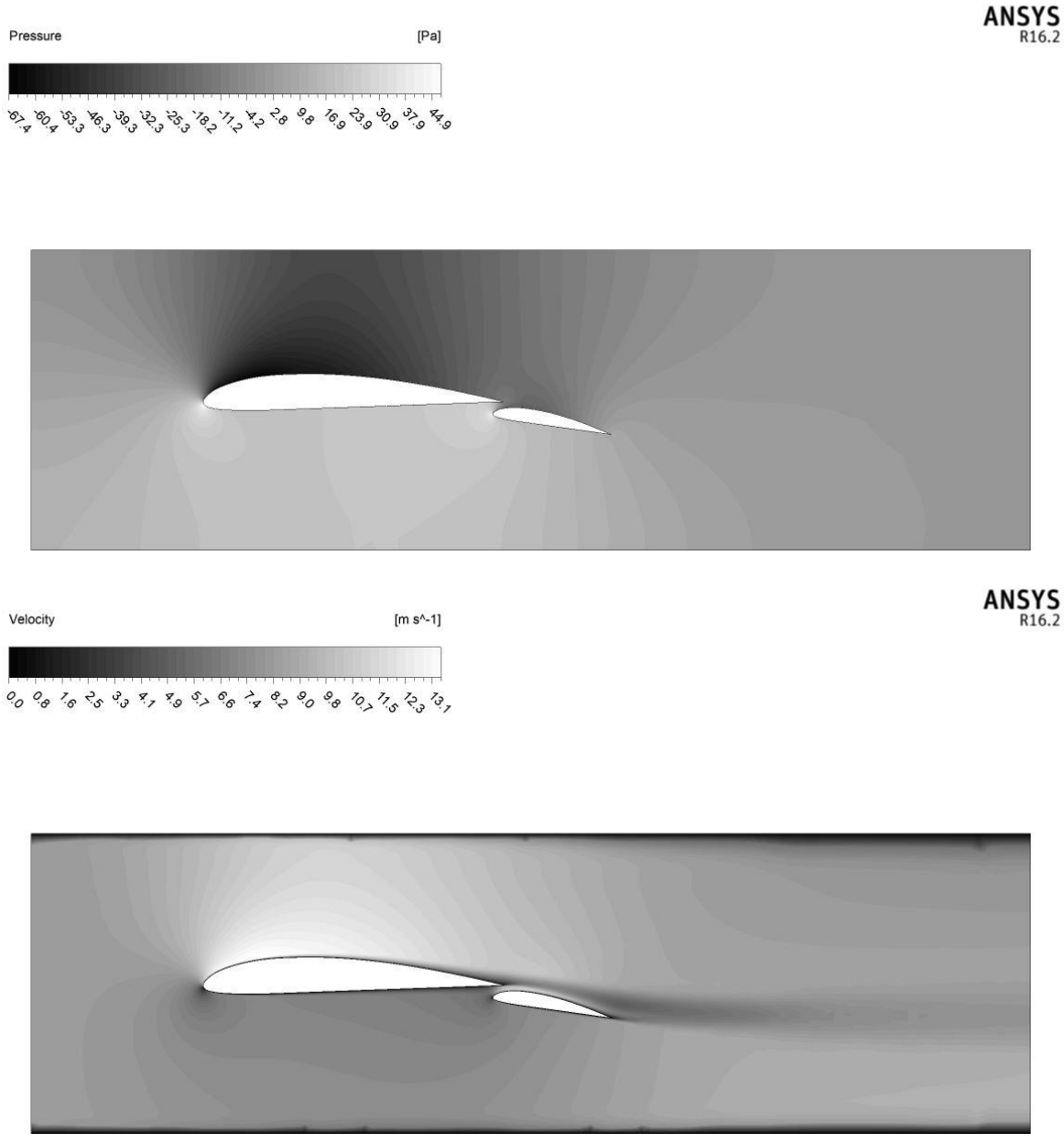

Fig 35: Pressure and Velocity distribution contour for profile 4 at 10 degrees of flap AOA

4.2.8 Double Element Profile 4 at 15 degrees Flap AOA

Further increase of AOA of the flap up to 15 degrees from the horizontal shows air flow separation starting from the trailing edge of the main element. This is unwanted because it creates a severe potential for the stall of the flap and adverse pressure gradient making it more of a disadvantage. Study of the airfoil profile beyond an AOA of 15 degrees would create enhanced boundary layer separation, hence the study is ended at the attack angle of 15 degrees.

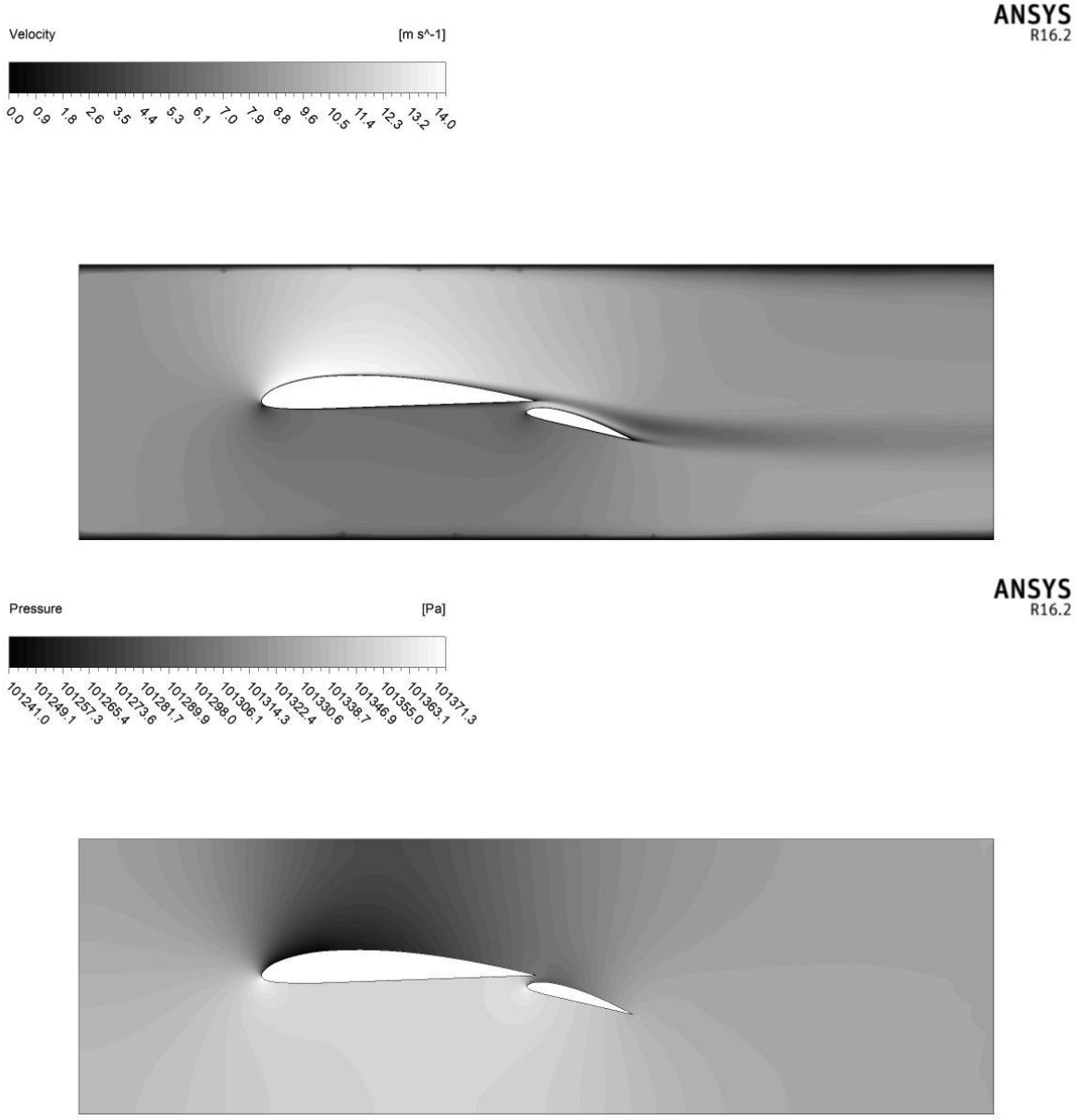

Fig 36: Pressure and Velocity distribution contour for profile 4 at 15 degrees of flap AOA

Chapter 5 Experimentation Setup

5.1 Fabrication of Double Element Clark Y Airfoil

A model of Clark Y airfoil was manufactured as discussed in designs mentioned in Chapter 3, section 3.1. The profile of the airfoil was extracted as co-ordinates from airfoil data base one can easily access. The CSV file was used to plot sketch of the profile using Solidworks and the sketch was then converted to DXF file for CNC cutting. CNC cutting was an automated process that favored higher degree of accuracy along with ease of manufacturing in comparison with other manufacturing techniques available. Airfoils are dimensionally sensitive systems and hence any method that would compromise such relative sizing was not prioritized. Medium Density Fiberboard (MDF), a kind of polished wood, of a thickness of 11mm was used as the material of choice for its ability to be smoothened without fracturing.

Twelve profiles of 150mm*11mm Clark Y was cut in a 11mm board initially. Later another set of 60mm*11mm scaled down profile was cut in a similar 11mm board that could act as a flap. The profiles were glued together as layers and were heavily polished to ensure minimum surface roughness.

Fig 37: Layer wise manufacture of airfoil profiles using automated CNC

The main idea of the airfoil system was to have a geometrically similar Clark Y wing, while also having higher degrees of freedom. Using screws as pivots, three degrees of freedom were achieved. Each degrees of movement would allow the elements of airfoil to achieve separate

angle of attack. This was done instead of fixing the location of elements so that versatility could be achieved in wind tunnel.

Fig 38: Final double-element airfoil system with 3 degrees of freedom

The objectives of fabricating the wing model was initially to visualize the air flow using smoke visualization method, followed by tuft flow visualization and acquire numeric data through laser intensive Particle Image Velocimetry (PIV) or pressure tapping.
With mentioned objectives, a total of 8 holes were drilled through the plane normal to the wings. This was done in order to stick tapping pipes through collect pressure data, which has also been mentioned in section 5.3.

5.2 Edibon EEE Wind Tunnel Setup

A cylindrical laboratory-based wind tunnel with dimension of 2000mm*540mm was available at Kathmandu University under ESTRL and was open to use for studies regarding effects of air flow patterns over turbines. It consisted of a long and narrow chamber that was equipped with a blower fan potential of generating streams of air at a maximum velocity of 11 m/s. Edibon EEE setup was a standalone wind tunnel powered by a 700-cfm centrifugal air pump, and was non-digitalized. The setup was initially installed in laboratory with a priority to study wind turbines, which is why the turbine model that came attached to the setup became a great hinderance within the study.

The wind tunnel set up included:

- Test section: The long and narrow chamber where the object is placed to be tested.
- Air Pump: The component that generates the airflow inside the tunnel. Inlet and outlet sections: The sections of the tunnel that allow air to enter and exit. Measuring instruments: Sensors and instruments used to measure the airflow properties such as velocity, pressure, temperature, etc.
- Data acquisition system: The system used to collect and store the data obtained from the measuring instruments.
- Control system: The system used to regulate the speed and direction of the airflow.

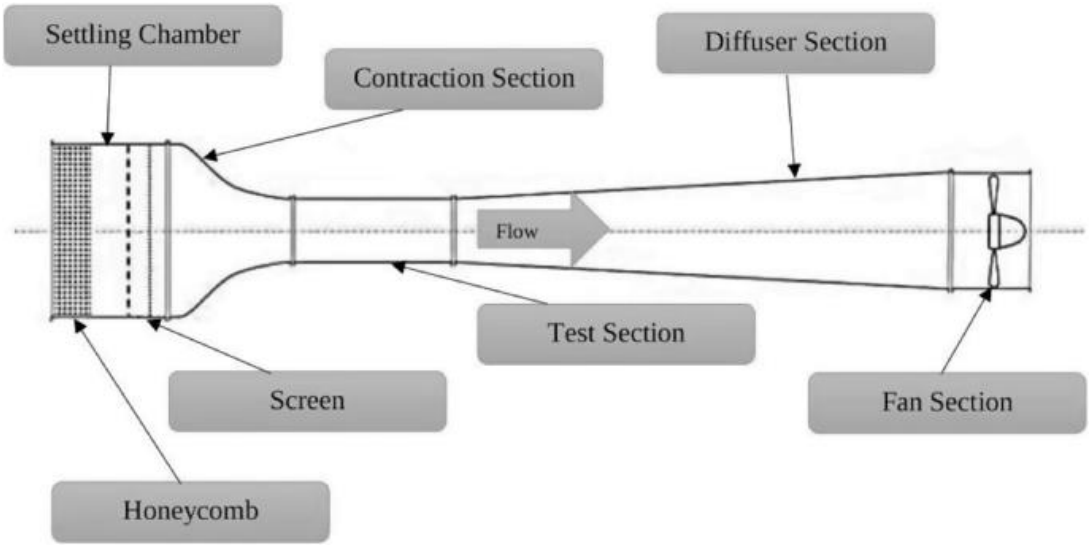

Fig: [38]

Fig 39: Edibon wind tunnel setup available at ESTRL, Kathmandu University

5.3 Scan valve Pressure Transducer

Pressure transducer is a device that is used to measure the pressure of a fluid or gas in a particular environment. It converts the pressure into an electrical signal, which can then be processed and analyzed by a computer or other measuring instrument. Pressure transducers are commonly used in wind tunnel testing to measure the air pressure distribution on an airfoil or any other object being tested. In the case of airfoil pressure measurement, pressure transducers are used to measure the pressure difference between the upper and lower surfaces of the airfoil at various points along its length. To measure the airfoil pressure distribution, pressure taps are installed on the surface of the airfoil at specific locations. These taps are small holes that are drilled into the surface of the airfoil and connected to a pressure transducer via small tubes. As air flows over the airfoil, the pressure at each tap is measured by the pressure transducer, and this data is recorded and analyzed. The pressure data obtained from the transducers can provide insights into the aerodynamic performance of the airfoil, including lift, drag, and other aerodynamic forces. The distribution of pressure over the surface of the airfoil can also be used to identify areas of low pressure, which can lead to the formation of vortices or other undesirable effects.

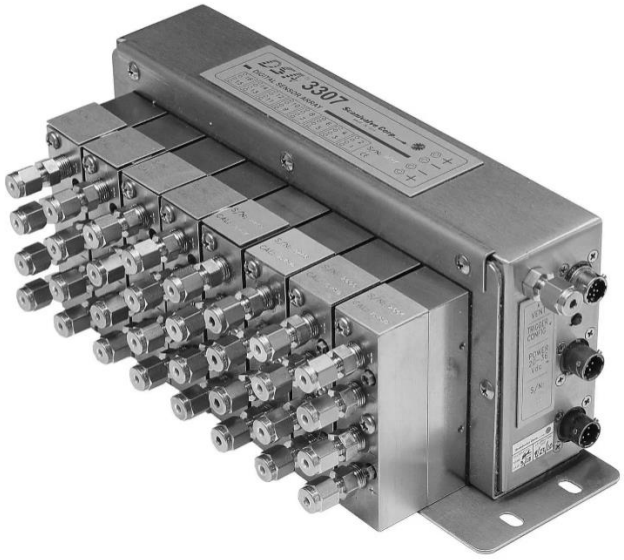

Fig 40: Channel pressure scanner, model no. DSA3207

A total of 14 pressure tapping sensors were available. Out of 14 sensors, only 8 were used for this study. Error tests were performed first in order to recognize its reliability. The standard atmospheric pressure as given by a chart in Yunus A. Cengel's Fluid Mechanics for an altitude

of 1400m (altitude of piloting location), was about 85.60 KPa. The data offered by pressure scanner three iterations averaged was 84.748 KPa. Hence the error of measurement was about 0.009%.

A total of 30 sets of data were acquired from the pressure transducers using taps, among which many were iterated for proper validation and reliability. A standalone software was used for the purpose that came along with the transducer. Data was exported in TXT file format and over 30 txt files were created over the period of data acquisition. The data obtained were severely fluctuated even at zero air flow, which was why averaging was done to proceed further.

5.4 Instrument Error

Scan valve pressure transducer possesses 14 pressure sensors. An initial test was performed to validate the accuracy and check the reliability of the instrument. It was also required for the calculations of lift coefficient to have static pressure values inside a wind tunnel operating at different velocities. Hence, the pressure transducer setup was installed inside the wind tunnel without connecting to the pressure taps. The data obtained from the 14 sensors for the same event and operating conditions are shown as follows. The data deviates by about 700 Pa between maximum and minimum values without showing convergence to a constant value.
The average values of static pressures inside wind tunnel were

- 84,711 Pa for velocity v = 4m/s
- 84, 699 Pa for velocity v = 6m/s
- 84, 618 Pa for velocity v = 8m/s
- 84, 670 Pa for velocity v = 10m/s

Whereas the average value for ambient pressure was 84,784 pascals. Since the velocity inside the tunnel is increasing for every iteration, pressure values are decreasing as they should be, except for flow at v=10m/s. The true value of static pressure at v=10m/s ought to be less than 84,618 Pa. Hence, through extrapolation of the trend, the value was replaced with 84,583 Pa which is a far more suited magnitude.

- 84, 583 Pa for velocity v = 10m/s

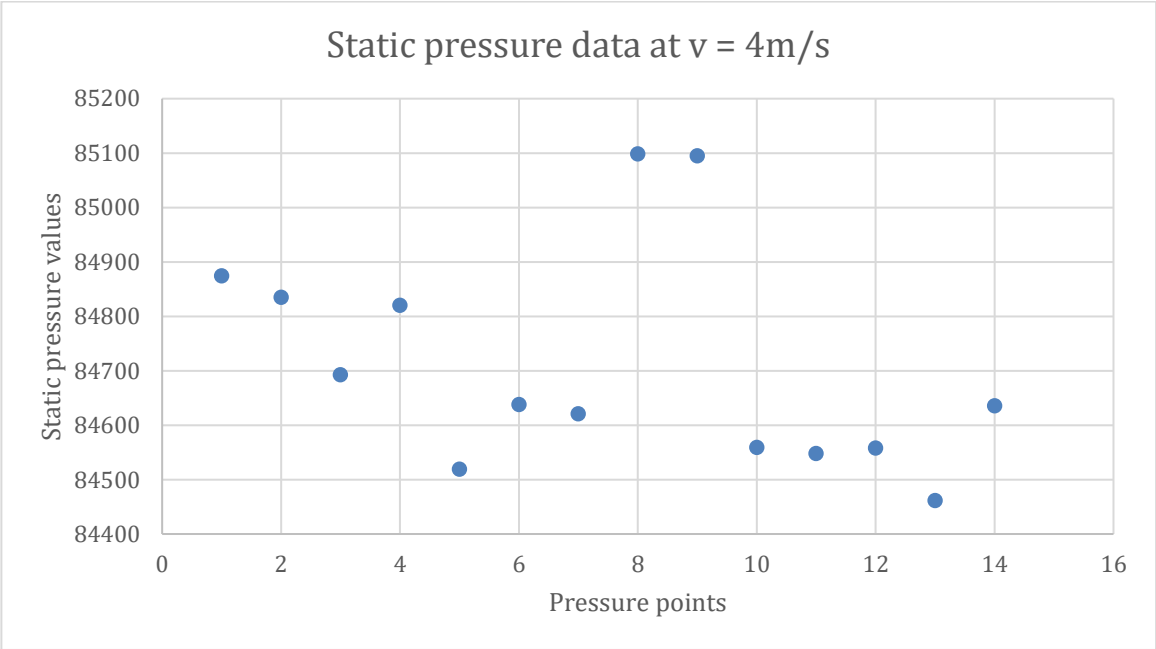

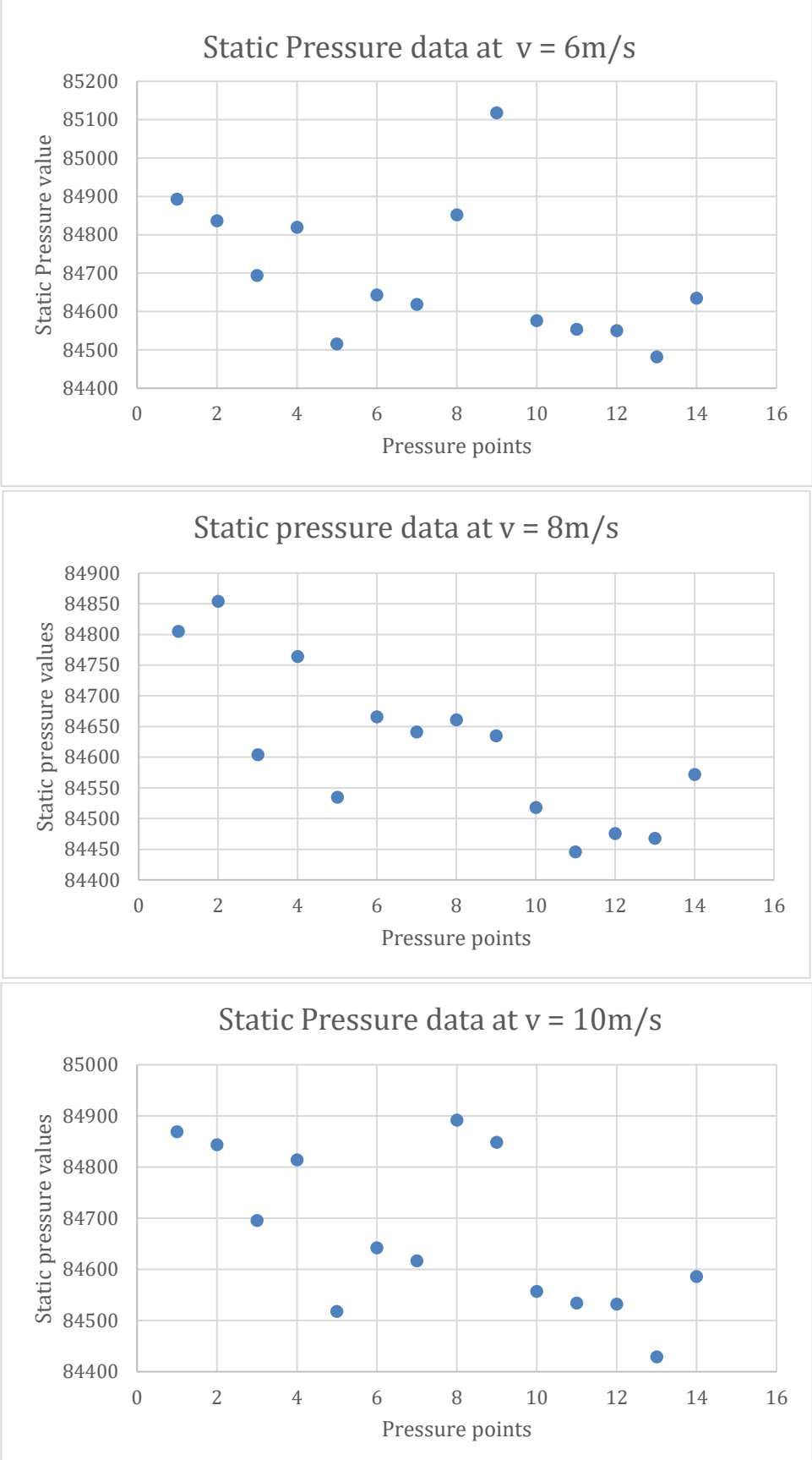

Fig 41: Deviation of values of same static pressure as a result of instrumental error for different velocities

5.5 Tuft Airflow Visualization

For the qualitative flow visualization on airfoil, tufts were used for their simplicity. Strings of approximate 1mm diameter were placed on the upper surface of the wing and in variation of speed and angle of attack, flow around the surface was anticipated. Strings were placed at 5 different rows as shown in figure 41 and were glued to the surface. Angle of attack and upstream velocity were varied to understand the boundary layer separation, turbulence wakes and formation of vortices.

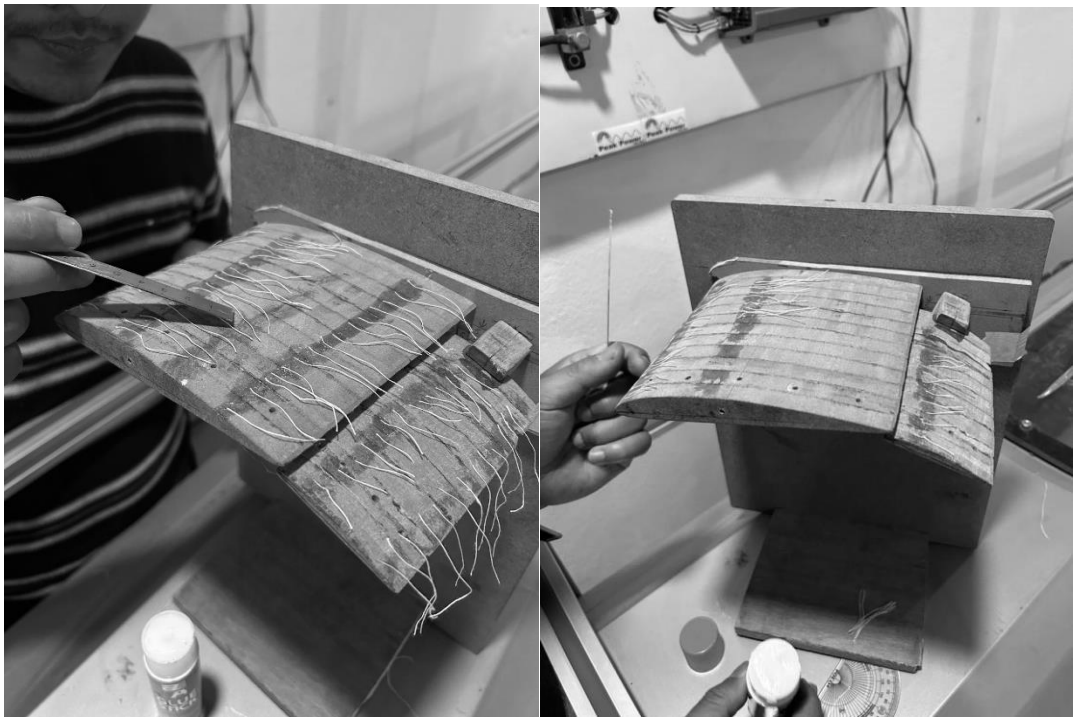

Fig 42: Placement of tufts at distances relative to the leading edge of the airfoil system

Chapter 6 Experimentation Results and Validation

6.1 Summary and Instrument error

By the end of chapter 5, multiple simulations and geometrical iterations were accomplished. The geometry details for the simulations are given as below.

i. Profile 1: With upper flap
ii. Profile 2: With lower flap
iii. Profile 3: With upper slat
iv. Profile 4: With lower slat
v. Domain details: 500mm*150mm

The geometries have been explained in details in section 3.2 for reference. Even with the availability of three degrees of freedom in the manufactured wing model, due to the presence of multiple profile orientations and tediousness, it was not deemed feasible to study all the orientations under the multi-element airfoils. Double elements were only a peek of the multi-element orientations; however, the intensive study required more time and effort than anticipated.

Hence, only few promising orientations such as the one with flaps were selected for experimentation. The experiment was performed in multiple methods as discussed with details in chapter 5.

6.2 Pressure Taps Over Airfoil Surfaces

Pressure tappings were set up on locations indicated as follows.

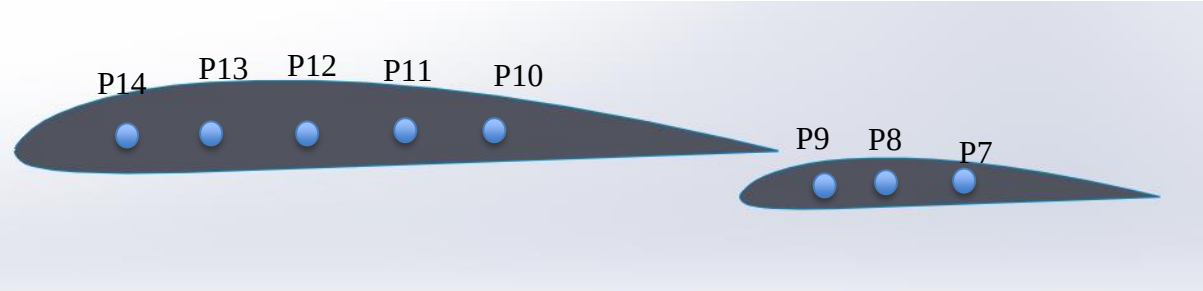

Fig 43: Taps at different locations relative to leading edge of the airfoil system

The tapping holes are replicated in figure 43. With a total of 8 taps, 5 lie in the main element of the size 150mm and 3 lie in the small element/flap, with 40% the size of main element, i.e. 60mm. The taps are indicated as P14, P13, P12, P11, P10, P9, P8, and P7 respectively starting from the 14^{th} sensor present in the scan valve with their positions set up in the form of x/c. The total length of the system is 150mm+60mm-5mm, where 5mm is subtracted because of negative overhang/overlap between main element and the flap. However, the positions are listed below.

- P14: 30mm from leading edge
- P13: 60mm from leading edge
- P12: 80mm from leading edge
- P11: 100mm from leading edge
- P10: 120mm from leading edge
- P9: 165mm from leading edge
- P8: 175mm from leading edge
- P7: 185mm from leading edge

The positions of the taps in terms of x/c are given as:

- P14: 0.2
- P13: 0.3
- P12: 0.4
- P11: 0.5
- P10: 0.6
- P9: 0.8
- P8: 0.85
- P7: 0.9

It should be noted that x/c positioning is relative in nature with 1 being trailing edge and 0 being the leading edge of the airfoil system. This has been discussed in section 4.3.

6.3 Pressure Readings and Data Tables

As previously mentioned, over 30 sets of data in the form of txt files were extracted. Each file contained about 1500 frames of data over 14 sensors, and collected within 20-time steps (each second counting as a time step). Data analysis part was harshly tedious and time consuming.

However, the data from the pressure transducer are placed in the tables as below.

6.3.1 For 0 degrees Flap AOA

Table 1: Pressure values and pressure coefficients for airfoil system at 0 degrees flap AOA

For 0 degrees AOA, ambient pressure = 84874								
	Pressure (upper surface) in pascals							
velocity (m/s)	P14	P13	P12	P11	P10	P9	P8	P7
4	84628	84496	84489	84480	84515	85591	84810	84611
6	84615	84490	84482	84464	84502	85570	84793	84599
8	84630	84503	84494	84484	84519	85578	84808	84624
10	84650	84509	84510	84493	84540	85584	84827	84634
	Pressure coefficient (upper surface)							
velocity (m/s)	P14	P13	P12	P11	P10	P9	P8	P7
4	-29.0	-44.6	-45.4	-46.4	-42.3	84.6	-7.6	-31.0
6	-13.6	-20.1	-20.5	-21.5	-19.5	36.5	-4.3	-14.4
8	-7.2	-10.9	-11.2	-11.5	-10.5	20.7	-1.9	-7.4
10	-4.2	-6.9	-6.9	-7.2	-6.3	13.4	-0.9	-4.5

By rule of thumb, it is obvious that for any airfoil, that pressure around the upper surface is comparatively lower than any other regions. Tap points P14 and P7 are close to leading and trailing edges respectively, whereas, tap points P13, P12 and P11 lie at mere central location where thickness of the airfoil dominates over the air flow.

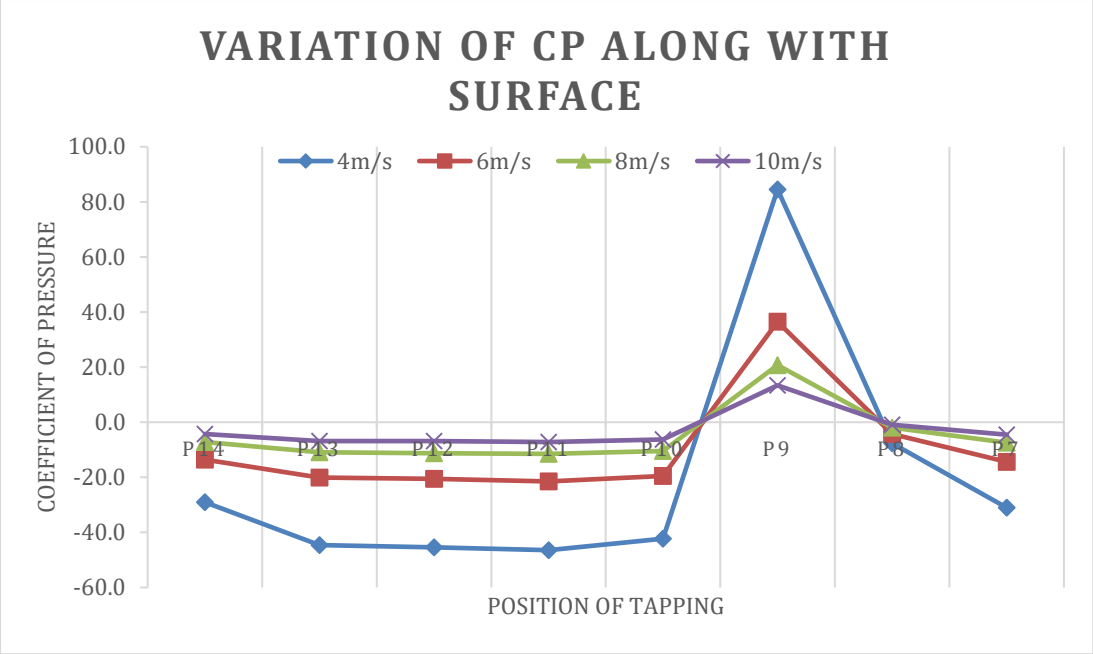

Fig 44: Graph of Cp vs tap position for 0 degrees flap AOA

Even though the pressure coefficients are supposed to be within the range of -1 to 1, the data obtained are far more ridicule in nature and hence, pressure coefficients vary from a minimum value of -46.4 at P11 (4m/s) to a maximum value of 84.6 at P9 (4 m/s) which isn't practically true unless some technical faults persist.

6.3.2 For 5 degrees Flap AOA

Table 2: Pressure values and pressure coefficients for airfoil system (upper surface) at 5 degrees flap AOA

For 5 degrees AOA								
	Pressure (upper surface)							
velocity (m/s)	P14	P13	P12	P11	P10	P9	P8	P7
4	84608	84520	84467	84450	84496	85801	84779	84589
6	84670	84482	84476	84497	84489	85802	84777	84621
8	84628	84468	84482	84472	84514	85585	84798	84611
10	84611	84515	84497	84490	84528	85551	84820	84628
	Pressure coefficient (upper surface)							
velocity (m/s)	P14	P13	P12	P11	P10	P9	P8	P7
4	-31.42	-41.80	-47.94	-50.06	-44.53	109.36	-11.21	-33.58
6	-10.71	-20.57	-20.88	-19.75	-20.16	48.63	-5.09	-13.27
8	-7.25	-11.96	-11.55	-11.86	-10.61	20.97	-2.25	-7.75
10	-4.95	-6.76	-7.11	-7.25	-6.52	12.77	-1.01	-4.63

Table 3: Pressure values and pressure coefficients for airfoil system (lower surface) at 5 degrees flap AOA

For 5 degrees AOA, ambient pressure = 84874								
	Pressure (lower surface) in pascals							
velocity (m/s)	P14	P13	P12	P11	P10	P9	P8	P7
4								
6								
8	84633	84505	84484	84481	84506	86175	84819	84592
10								
	Pressure coefficient (lower surface)							
velocity (m/s)	P14	P13	P12	P11	P10	P9	P8	P7
4								
6								
8	-7.09	-10.89	-11.51	-11.59	-10.84	38.34	-1.63	-8.31
10								

Note* Empty boxes means absence of data

Table 4: Lift coefficient values for airfoil system at 5 degrees flap AOA

velocity (m/s)	Lift coefficient								
	P14	P13	P12	P11	P10	P9	P8	P7	Average Cl
4									
6									
8	0.163	1.067	0.033	0.270	-0.231	17.369	0.617	-0.560	0.194
10									

From the data collected, average lift coefficient over the surface was found to be 0.194, excluding highly deviated value at P9. Cl was calculated by subtracting Cp of upper surface from Cp of lower surface.

i.e. $C_L(x) = Cp\ (lower) - Cp\ (upper)$

In conclusion, lift generated at 5 degrees flap AOA is positive in nature.

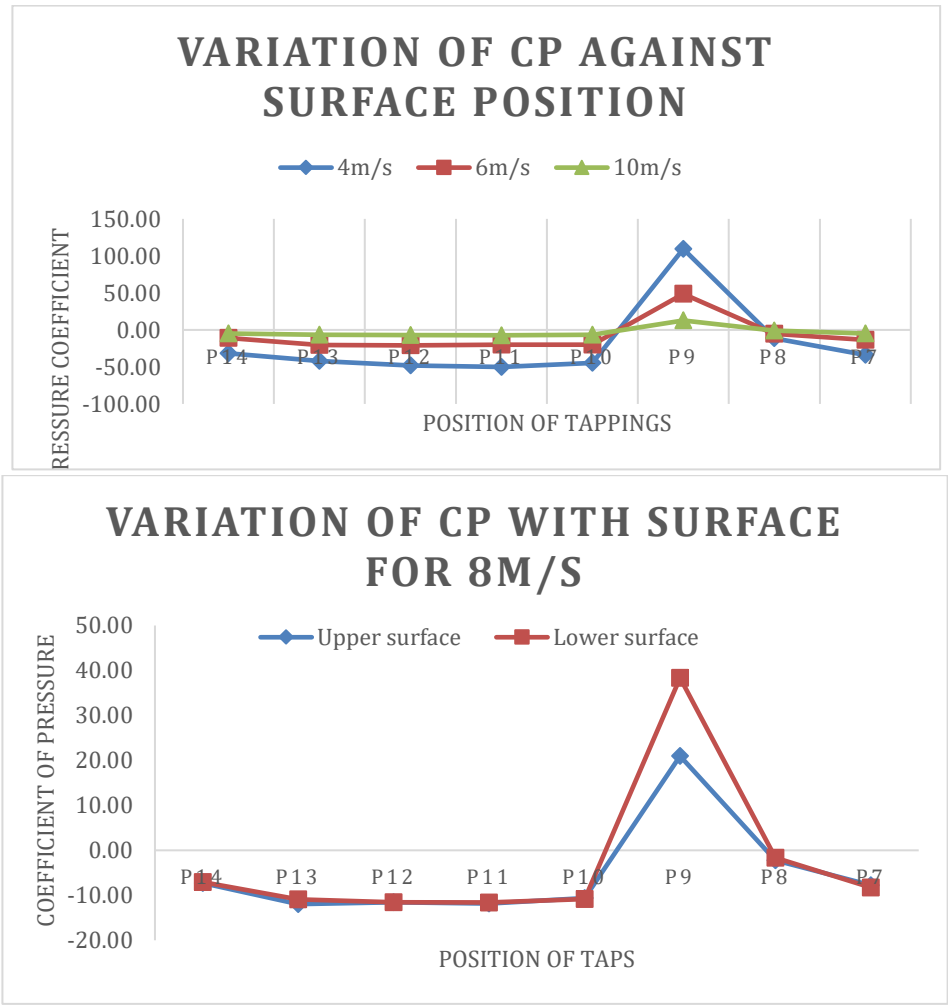

Fig 45: Graph of Cp vs tap position for 5 degrees flap AOA

6.3.3 For 10 degrees Flap AOA

Table 5: Pressure values and pressure coefficients for airfoil system (upper surface) at 10 degrees flap AOA

For 10 degrees AOA								
	Pressure (upper surface) in pascals							
velocity (m/s)	P14	P13	P12	P11	P10	P9	P8	P7
4								
6								
8	84614	84513	84488	84473	84516	85646	84806	84609
10								
	Pressure coefficient (upper surface)							
velocity (m/s)	P14	P13	P12	P11	P10	P9	P8	P7
4								
6								
8	-7.67	-10.64	-11.39	-11.84	-10.54	22.75	-2.01	-7.81
10								

Table 6: Pressure values and pressure coefficients for airfoil system (lower surface) at 10 degrees flap AOA

For 10 degrees AOA								
	Pressure (lower surface) in pascals							
velocity (m/s)	P14	P13	P12	P11	P10	P9	P8	P7
4								
6								
8	84611	84492	84486	84477	84500	86185	84811	84583
10								
	Pressure coefficient (lower surface)							
velocity (m/s)	P14	P13	P12	P11	P10	P9	P8	P7
4								
6								
8	-7.76	-11.25	-11.44	-11.71	-11.03	38.64	-1.87	-8.57
10								

Note* Empty boxes means absence of data

Table 7: Lift coefficient values for airfoil system at 10 degrees flap AOA

velocity (m/s)	Lift coefficient								
	P14	P13	P12	P11	P10	P9	P8	P7	Average Cl
4									
6									
8	-0.089	-0.614	-0.046	0.128	-0.489	15.891	0.142	-0.764	-0.248
10									

For the flap AOA of 10 degrees, C_L obtained is negative in nature. Though this is not a favorable scenario for an airfoil system, it might have occurred as a result of error in pressure data, or, it might be because the airfoil system began to stall somewhere around 5 and 10 degrees of flap AOA. Simulation results too showed boundary separation characteristics at 10 and 15 degrees of AOA followed by tuft flow visualization that will be discussed in upcoming sections.

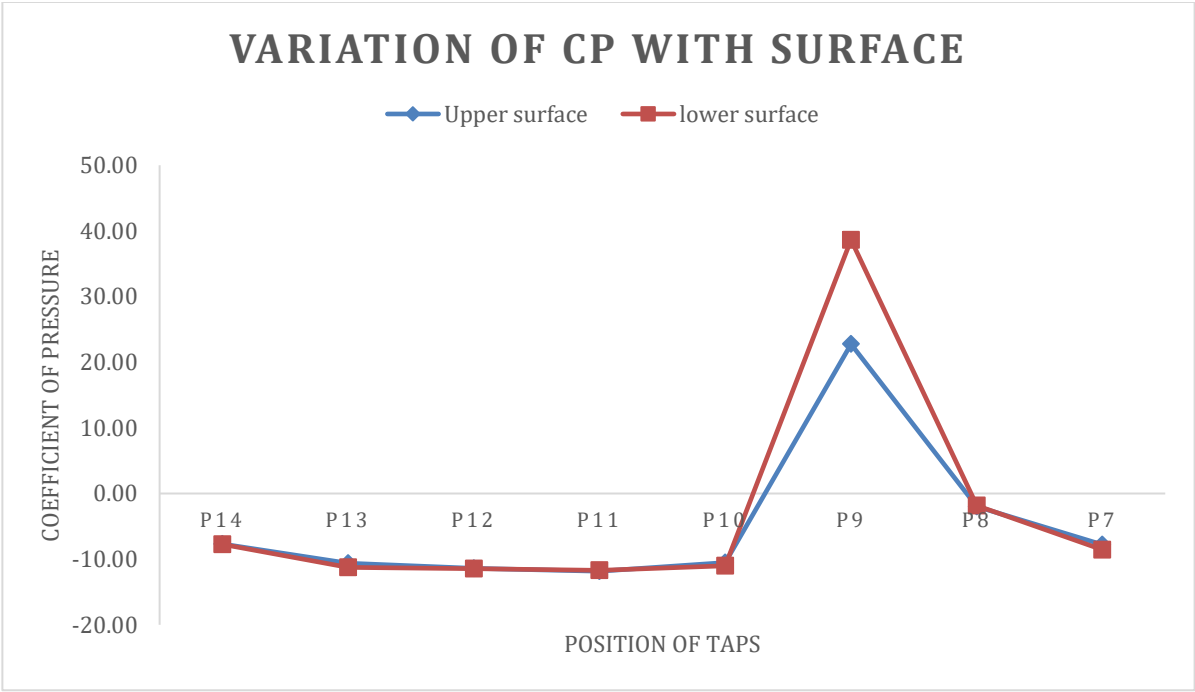

Fig 46: Graph of Cp vs tap position for 5 degrees flap AOA

6.3.4 For 15 degrees Flap AOA

Table 8: Pressure values and pressure coefficients for airfoil system (upper surface) at 15 degrees flap AOA

For 15 degrees AOA, ambient pressure = 84874								
	Pressure (upper surface) in pascals							
velocity (m/s)	P14	P13	P12	P11	P10	P9	P8	P7
4								
6								
8	84628	84520	84489	84465	84513	85721	84804	84610
10								
	Pressure coefficient (upper surface)							
velocity (m/s)	P14	P13	P12	P11	P10	P9	P8	P7
4								
6								
8	-7.25	-10.44	-11.35	-12.06	-10.64	24.97	-2.06	-7.78
10								

Table 9: Pressure values and pressure coefficients for airfoil system (upper surface) at 15 degrees flap AOA

For 15 degrees AOA, ambient pressure = 84874								
	Pressure (lower surface) in pascals							
velocity (m/s)	P14	P13	P12	P11	P10	P9	P8	P7
4								
6								
8	84613	84507	84456	84464	84509	86055	84823	84593
10								
	Pressure coefficient (lower surface)							
velocity (m/s)	P14	P13	P12	P11	P10	P9	P8	P7
4								
6								
8	-7.71	-10.82	-12.31	-12.10	-10.77	34.81	-1.49	-8.29
10								

Note* Empty boxes means absence of data

Table 10: Lift coefficients for airfoil system (upper surface) at 15 degrees flap AOA

velocity (m/s)	Lift coefficient								
	P14	P13	P12	P11	P10	P9	P8	P7	Average Cl
4									
6									
8	-0.455	-0.387	-0.959	-0.043	-0.128	9.839	0.571	-0.504	-0.272
10									

Similar to 10 degrees flap attack angle, the coefficient of lift is negative in nature indicating the stall. The exact reason of such negative value is unknown, but the authors anticipate it as the effect of stall, where the wings no longer produce lift after certain angle of attack.

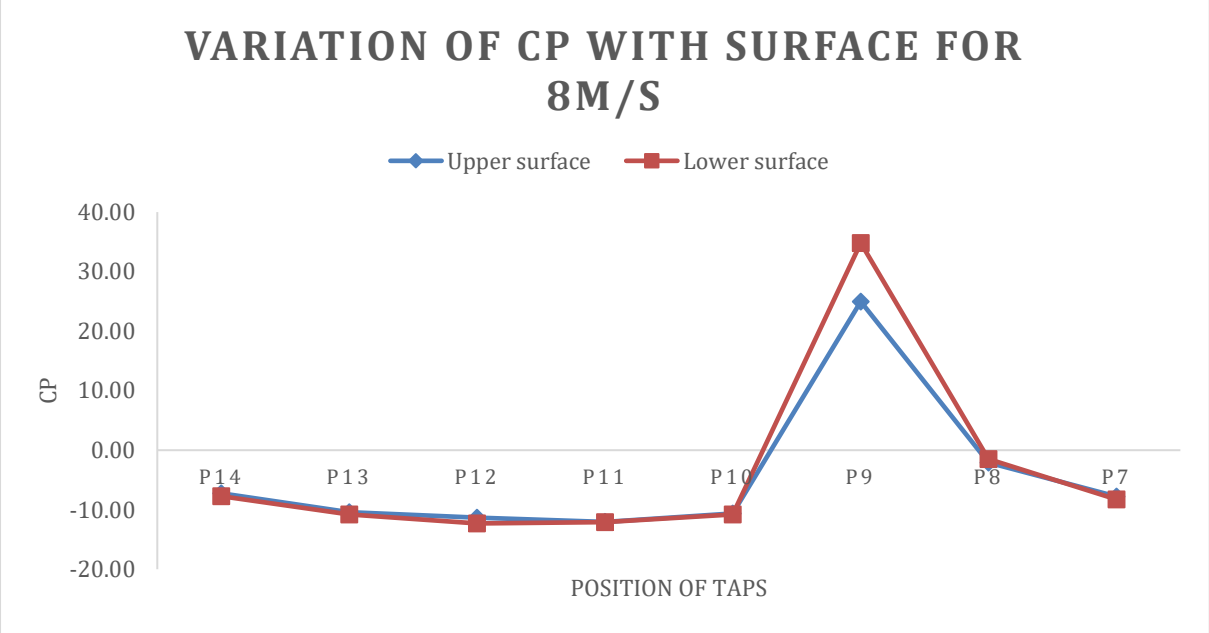

Fig 47: Graph of Cp vs tap position for 5 degrees flap AOA

6.4 Validation from Tufts

As discussed in previous sections, strings were placed as tufts to validate the flow around the airfoil. Details on position of tufts are as follows.

- Tuft row 1: 0.15 from leading edge
- Tuft row 2: 0.35 from leading edge
- Tuft row 3: 0.55 from leading edge
- Tuft row 4: 0.7 from leading edge
- Tuft row 5: 0.9 from leading edge

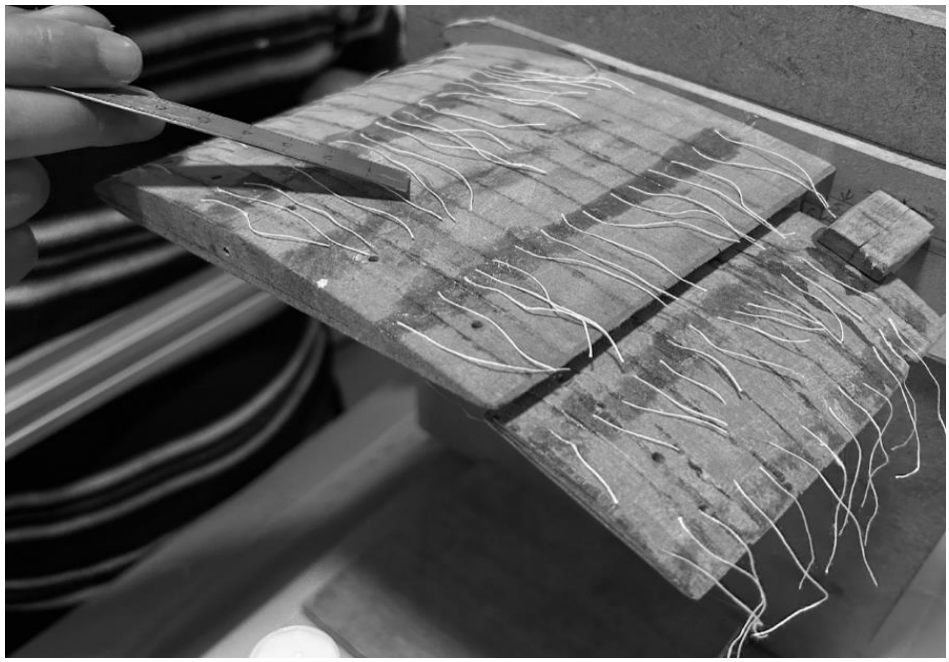

Fig 48: Tufts and its positions

6.4.1 Front element at -5° AOA, Back element at 15° AOA at speed of 4m/s

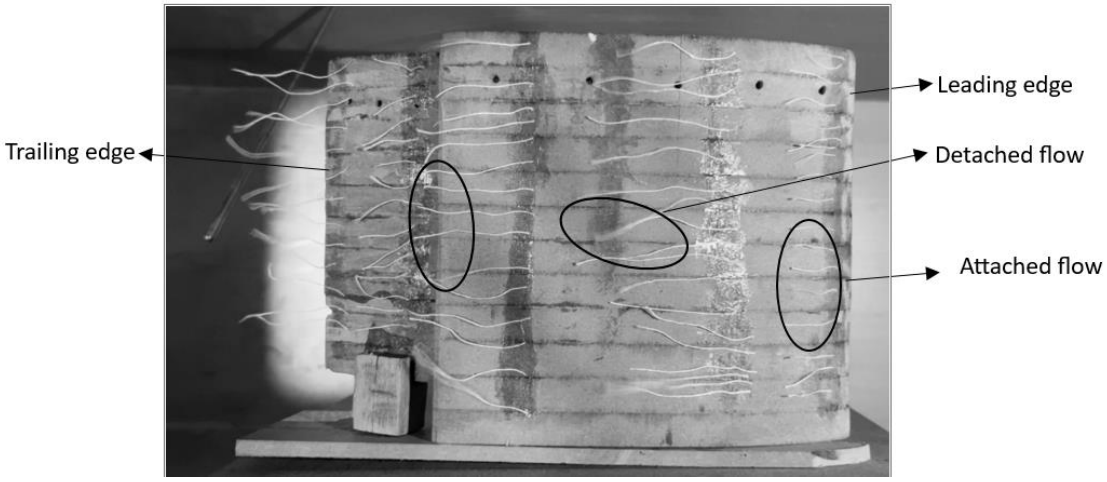

Fig 49: Wiggling tufts representing boundary separation

When front main element is placed slightly lower at an angle of -5 degrees, and rear element at 15 degrees, flow seems to detach from the surface and create turbulence. Such boundary layer separation of air might be the cause of stall and negative coefficient of lift. On further questioning, the overall body could be blamed for occurrence of such behaviors: rough surface, or even inaccurate geometry.

6.4.2 Front element at 0 degrees AOA, back element at 5 degrees AOA at 4m/s

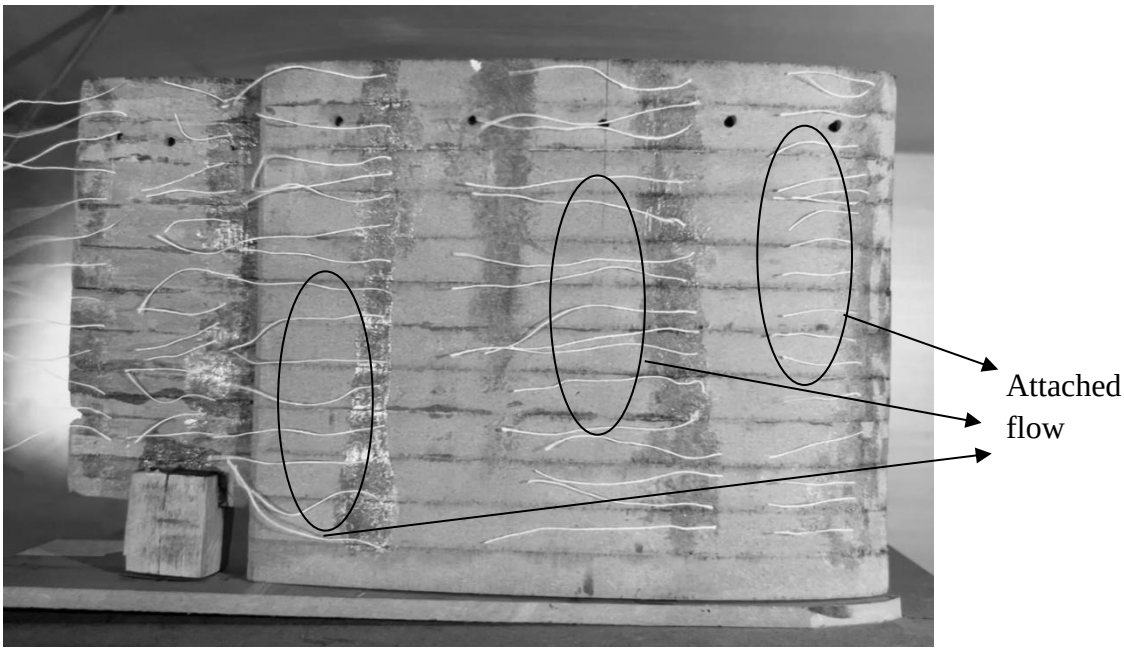

Fig 50: Tuft visualization of attached flow to some extent

At minimum flap AOA of 5 degrees and at a velocity of 4m/s, the flow was seen somewhat attached and laminar up to a relative position of 0.55 from leading edge. A theory concerned to such attached flow behavior is that at 4 m/s, the flow is relatively less turbulent than at higher velocities, which could have been a possible reason for streamlined tufts.

6.4.3 Front element at 0 degrees AOA, back element at 5 degrees AOA at 8m/s

At flap AOA of 5 degrees and at a velocity of 8 m/s, the flow was starting to get dettached from the airfoil surface starting at a relative position of 0.35 from the leading edge.

6.4.4 Front element -5° AOA, Back element at 15° AOA at speed of 8m/s

Results are similar at air flow speed of 8m/s. Air flow separation is seen starting somewhere at x/c of 0.35. This is also true for tests done at a velocity of 10 m/s.

6.4.5 Front element at 15° AOA, Back element at 15° AOA at speed of 8m/s

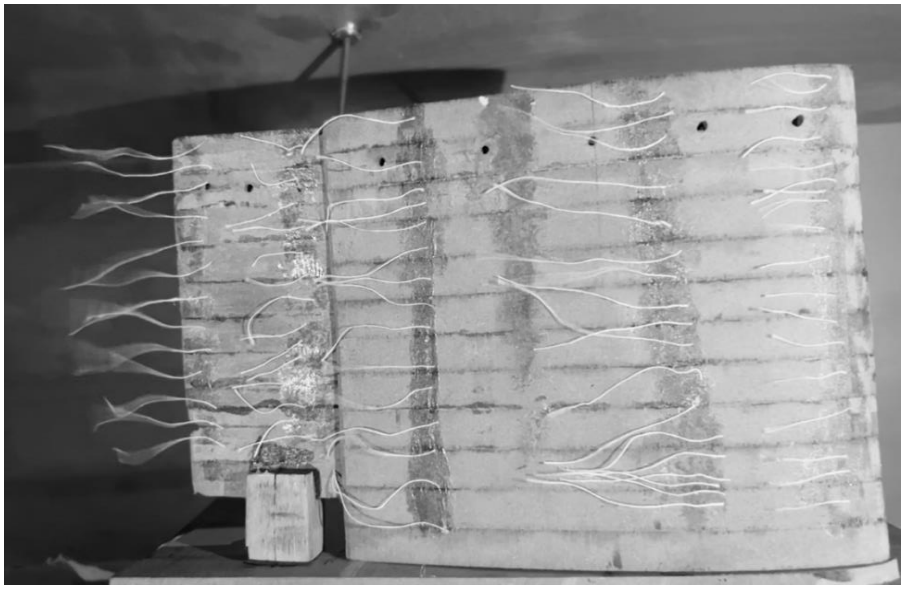

At angle of attack of 15 degrees for both the elements, along with the velocity of 8m/s, flow separation with the turbulent movement of string at chord length of 0.1 was observed.

Chapter 7 Conclusion

The research concludes on a standing that double element wings offer poor performance for flap AOA greater than 5 degrees. A thorough explanation of multi-element airfoils for speeds as low as 8 m/s was done and theoretical and experimental research on double-element airfoils were summarized. The unbroken Clark Y airfoil geometries, layered one after other with a gap of 5mm and an overhang of 6mm, were studied successfully. The study's primary goals to examine the flow fields produced by double-element airfoils at various orientations was also accomplished and, were validated using various experimental techniques like pressure tapping for quantitative authentication and tuft flow visualization for qualitative justification.

Glossary: Flight Mechanics

Adverse pressure gradient	: Pressure difference between upwash and downwash stream of air that causes the air velocity to reduce and detach from the surface
Angle of attack	: Angle between chord line of airfoil and direction of airflow
Aspect ratio	: Ratio of wingspan to its chord length
Bound vortex	: Vortex bound to the wing surface
Camber	: Vertical distance from center to the highest peak of an airfoil
Chord	: Length of the wing
Coanda effect	: Phenomenon in which a stream of moving fluid attaches itself to a nearby surface
Cove region	: Region behind slate of a multi-element wing
Downstream	: Air that flows away from the airfoil (Downwash)
Edge vortices	: Vortices formed at the leading and trailing edges
End plates	: Plates that prevent the formation of end point vortices in wings that would otherwise induce drag. Also called as Side fins
Gurney flaps	: Additional wing element placed behind the lift creating airfoil
Incidence	: Angle between chord of wing at centerline and horizontal
Leading edge	: Front edge of the airfoil that comes in contact with air as it moves
Laminar transition bubble	: A region of low-pressure zone formed on the surface of airfoil caused due to flow separation and reattachment, occurred in laminar flows.

Planform area	: Surface area of an airfoil
Slate	: First element of an optimized multi-element airfoil
Span	: Width of the wing
Stall	: A phenomena when airfoil stops generating lift when certain AoA limit is surpassed
Trailing edge	: Back edge of the airfoil
Upstream	: Air that flows towards the airfoil (Upwash)
Vortex breakdown	: Complex phenomenon described as abrupt and drastic change of structure that sometimes occur in a swirling flow
Vortex filament	: Imaginary spatial curve that induces rotary flow in the space through which vortices pass
Vortex shedding	: Leaving behind vortices in the wake region of airfoil

Glossary: ANSYS and Computational Fluid Dynamics

Adaption : A technique useful in improving overall mesh quality. The solution-adaptive mesh refinement feature of ANSYS FLUENT allows you to refine and/or coarsen your mesh based on geometric and numerical solution data. In addition, ANSYS FLUENT provides tools for creating and viewing adaption fields customized to particular applications.

Case files : Files that contain the mesh, boundary conditions, and solution parameters for a problem. A case file also contains the information about the user interface and graphics environment.

Cell types : The various shapes or units that constitute the base elements of a mesh. ANSYS FLUENT can use meshes comprised of tetrahedral, hexahedral, pyramid, wedge, or polyhedral cells (or a combination of these).

Console : The console is part of the ANSYS FLUENT application window that allows for text command input and the display of information.

Convergence : The point at which the solution is no longer changing with each successive iteration. Convergence criteria, along with a reduction in residuals, also help in determining when a solution is complete. Convergence criteria are pre-set conditions on the residuals that indicate that a certain level of convergence has been achieved. If the residuals for all problem variables fall below the convergence criteria but are still in decline, the solution is still changing to a greater or lesser degree. A better indicator occurs when the residuals flatten in a traditional residual plot (of residual value vs. iteration). This point, sometimes referred to as convergence at the level of machine accuracy, takes time to reach, however, and may be beyond your needs. For this reason, alternative tools such as reports of forces, heat balances, or mass balances can be used instead.

Cortex : A utility that manages ANSYS FLUENT's user interface and basic graphical functions.

Data files : Files that contain the values of the flow field in each grid element and the convergence history (residuals) for that flow field.

Dialog boxes : The separate windows that are used like forms to perform input tasks. Each dialog box is unique and employs various types of input controls that make up the form.

Discretization : The act of replacing the differential equations that govern fluid flow with a set of algebraic equations that are solved at distinct points.

Mesh : A collection of points representing the flow field, where the equations of fluid motion (and temperature, if relevant) are calculated.

Model : Numerical algorithms that approximate physical phenomenon (e.g., turbulence).

Node : The distinct points of a mesh at which the equations of fluid motion are solved.

Postprocessing: The act of analyzing the numerical results of your CFD simulation using reports, integrals, and graphical analysis tools such as contour plots, animations, etc.

Residuals : The small imbalance that is created during the course of the iterative solution algorithm. This imbalance in each cell is a small, non-zero value that, under normal circumstances, decreases as the solution progresses.

Skewness : The difference between the shape of the cell and the shape of an equilateral cell of equivalent volume. Highly skewed cells can decrease accuracy and destabilize the solution.

Solvers : ANSYS FLUENT has two distinct solvers, based on numerical precision (single-precision vs. double-precision). Within each of these categories, there are solver formulations: pressure based; density based explicit; and density based implicit.

REFERENCES

[1] S. C. Kachare, “A CFD Study of a Multi-Element Front Wing for a Formula One Racing Car”.

[2] S. Klausmeyer, M. Papadakis, and J. Lin, “A flow physics study of vortex generators on a multi-element airfoil,” in *34th Aerospace Sciences Meeting and Exhibit*, Reno,NV,U.S.A., Jan. 1996. doi: 10.2514/6.1996-548.

[3] A. Seeni, “A theory on understanding aerodynamic phenomena of airfoils and the significance of airfoil’s thickness on lift and drag,” *INCAS BULLETIN*, vol. 14, no. 3, pp. 101–110, Sep. 2022, doi: 10.13111/2066-8201.2022.14.3.9.

[4] N. M. Triet, N. N. Viet, and P. M. Thang, “Aerodynamic Analysis of Aircraft Wing,” vol. 31, no. 2, 2015.

[5] T. J. Mueller and J. S “Aerodynamics of multi-element wings in ground effect.”

[6] B. V Bhumi, R. Malhotra, R. Pandey “Airfoil design.” History and basic ideas of airfoils

[7] “Classical Aerodynamics.” [online pdf]

[8] M. Drela, “Design and optimization method for multi-element airfoils,” in *Aerospace Design Conference*, Irvine,CA,U.S.A., Feb. 1993. doi: 10.2514/6.1993-969.

[9] D. P. Coiro, F. Nicolosi, and F. Grasso, “Design and Testing of a Multi-Element Airfoil for Short-Takeoff-and-Landing Ultralight Aircraft,” *Journal of Aircraft*, vol. 46, no. 5, pp. 1795–1807, Sep. 2009, doi: 10.2514/1.43429.

[10] S. Anand, A. Pandey, A. Sharma, and C. R. Kini, “EFFECT OF TRAILING EDGE ROUNDNESS ON FX 63-137 AND SELIG S1223 AIRFOIL,” vol. 12, no. 19, 2017.

[11] Q. Qu, B. Ju, L. Huang, P. Liu, and R. K. Agarwal, “Flow Physics of a Multi-Element Airfoil in Ground Effect,” in *54th AIAA Aerospace Sciences Meeting*, San Diego, California, USA, Jan. 2016. doi: 10.2514/6.2016-0856.

[12] Aeronautics Research Mission Directorate, Museum in a box “*Principles of Flight*” Grade k-12

[13] M. Jahanmiri, “Laminar Separation Bubble: Its Structure, Dynamics and Control”.

[14] B. C. Khoo, “Letter: A note on flow characterization of the FX63-137 airfoil at low Reynolds number using oil-film interferometry technique,” *Physics of Fluids*, vol. 30, no. 10, p. 101701, Oct. 2018, doi: 10.1063/1.5052233.

[15] A. Pelletier and T. J. Mueller, “Low Reynolds Number Aerodynamics of Low-Aspect-Ratio, Thin/Flat/Cambered-Plate Wings,” *Journal of Aircraft*, vol. 37, no. 5, pp. 825–832, Sep. 2000, doi: 10.2514/2.2676.

[16] P. J. Ambhore and S. Mali, “Multi Element Wing Analysis”.

[17] R. Ranzenbach, J. Barlow, R. Diaz, R. Ranzenbach, J. Barlow, and R. Diaz, “Multi-element airfoil in ground effect - An experimental and computational study,” in *15th Applied Aerodynamics Conference*, Atlanta,GA,U.S.A., Jun. 1997. doi: 10.2514/6.1997-2238.

[18] W. Valarezo, C. Dominik, R. Mcghee, W. Goodman, and K. Paschal, “Multi-element airfoil optimization for maximum lift at high Reynoldsnumbers,” in *9th Applied Aerodynamics Conference*, Baltimore,MD,U.S.A., Sep. 1991. doi: 10.2514/6.1991-3332.

[19] S. Kim, J. J. Alonso, and A. Jameson, “Multi-Element High-Lift Configuration Design Optimization Using Viscous Continuous Adjoint Method,” *Journal of Aircraft*, vol. 41, no. 5, pp. 1082–1097, Sep. 2004, doi: 10.2514/1.17.

[20] “National Advisory Committee for Aeronautics: Motion of Fluids with very little viscosity.” [Online]. Available: https://ntrs.nasa.gov/api/citations/19930090813/downloads/19930090813.pdf

[21] J. O. M. Lucci, “Potential Flow Theory”.

[22] AH Techt. “Potential Flow Theory.”

[23] B. W. Pomeroy, J. M. Diebold, P. J. Ansell, and M. S. Selig, “Study of Burst Wakes in a Multi-Element Airfoil Flowfield,” *AIAA Journal*, vol. 52, no. 4, pp. 821–831, Apr. 2014, doi: 10.2514/1.J052680.

[24] C. P. van Dam, “The aerodynamic design of multi-element high-lift systems for transport airplanes,” *Progress in Aerospace Sciences*, vol. 38, no. 2, pp. 101–144, Feb. 2002, doi: 10.1016/S0376-0421(02)00002-7.

[25] Gaurang GatlewarGaurang Gatlewar 10722 gold badges22 silver badges77 bronze badges, FedericoFederico 31.9k1717 gold badges132132 silver badges179179 bronze badges and Peter KämpfPeter Kämpf 223k1717 gold badges572572 silver badges899899 bronze badges (1961) *How to plot the pressure distribution over an airfoil?*, *Aviation Stack Exchange*. Available at: https://aviation.stackexchange.com/questions/5230/how-to-plot-the-pressure-distribution-over-an-airfoil (Accessed: January 3, 2023). source for image on page 12

[26] Circulation around a wing. Available at: https://webarchive.library.unt.edu/eot2008/20080923064640/http:/centennialofflight.gov/essay/Theories_of_Flight/Airfoils/TH13G4.htm (Accessed: January 3, 2023). Source for image on page 13

[27] *Creative Commons License Deed* (no date) *Creative Commons - Attribution-ShareAlike 3.0 Unported - CC BY-SA 3.0*. Available at: https://creativecommons.org/licenses/by-sa/3.0/ (Accessed: January 3, 2023). source for image on page 17

[28] *Creative Commons License Deed* (no date) *Creative Commons - Attribution-ShareAlike 3.0 Unported - CC BY-SA 3.0*. Available at: https://creativecommons.org/licenses/by-sa/3.0/ (Accessed: January 3, 2023). source for second image on page 17

[29] "Aerospaceweb.org | ask US - NACA airfoil series." [Online]. Available: http://www.aerospaceweb.org/question//airfoils/q0041.shtml. [Accessed: 03-Jan-2023] Online pdf: source

[30] Airfoil geometry.svg (no date) Wikimedia Commons. Available at: https://commons.wikimedia.org/wiki/File:Airfoil_geometry.svg (Accessed: January 3, 2023). Online pdf: source

[31] NACA Airfoils on 'NASA TV', online image: https://www.nasa.gov/image-feature/langley/100/naca-airfoils

[32] *NACA 6412 (NACA6412-IL)*. Available at: http://airfoiltools.com/airfoil/details?airfoil=naca6412-il (Accessed: January 3, 2023). http://airfoiltools.com/airfoil/details?airfoil=naca6412-il

[32] Tarun B Patel, "An analysis of lift and drag forces of NACA airfoils"

[33] Airfoil Classification. (n.d.) An Illustrated Dictionary of Aviation. (2005). Retrieved January 31 2023 from https://encyclopedia2.thefreedictionary.com/airfoil+classification

[34] Yunus A. Cengel, "*Dimensional Analysis and Modeling",* Fluid Mechanics Ch.7

[35] ANSYS Inc., Southpointe, "*ANSYS Meshing User's Guide*", 275 Technology drive, Canonsberg, 2010 [pdf]

[36] Takeo Kajishima, Kunihiko Taira, "*Computational Fluid Dynamics*", Department of Mechanical Engineering, University of Osaka

[37] Shreyansh Kanshal, "*Flow Visualization Techniques: Pressure Sensitive Paints*", Aircraft Nerds [online article]. Available at https://www.aircraftnerds.com/2018/08/flow-visualization-technique-pressure-sensitive-paints.html

[38] Sailesh Chitrakar, "*Solutions on Algorithms for Pressure Velocity Coupling in Steady Flows*", Kathmandu University, Department of Mechanical Engineering, p12-p28 [Lecture notes]

[39] "Design of Low Speed Smoke Visualization Tunnel", Springerlink [Online webpage] Available at: https://link.springer.com/chapter/10.1007/978-981-16-7909-4_60